III International Conference and School
"Synthesis, Structure, and Properties of High-Entropy Materials"
October 11-15, 2021

№29

ozerov@bsu.edu.ru

Ozerov M.S., Stepanov N.D., Zherebtsov S.V. MICROSTRUCTURE AND MECHANICAL PROPERTIES OF THE MEDIUM-ENTROPY NBTIZR ALLOY-BASED COMPOSITE, REINFORCED WITH BORIDE PARTICLES

The aim: Investigation of microstructure and mechanical properties of NbTiZr/(NbTiZr)B composite obtained by vacuum arc remelting process

Method of obtaining

Vacuum arc remelting

Buehler Arc Melter 200 (Германия)

Microstructure

TiNbZr – 0.2 % mass. TiB

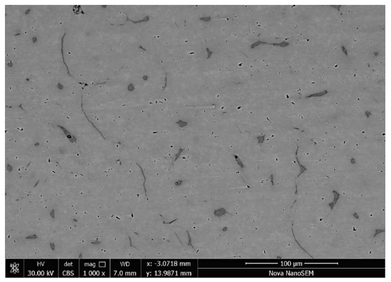

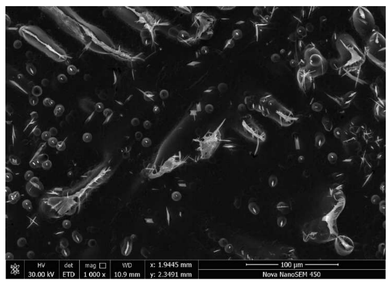

TiNbZr – 2 % mass. TiB

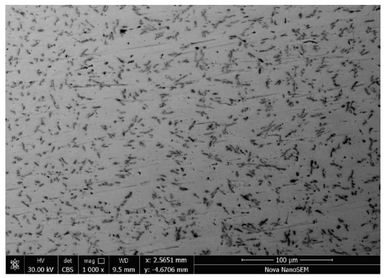

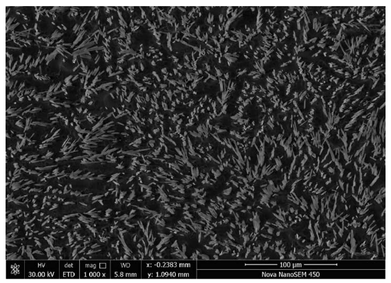

TiNbZr – 4.41 % mass. TiB

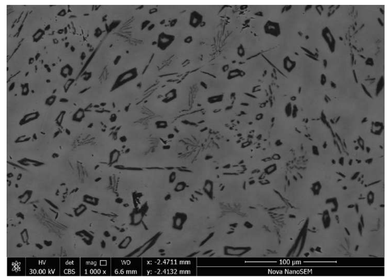

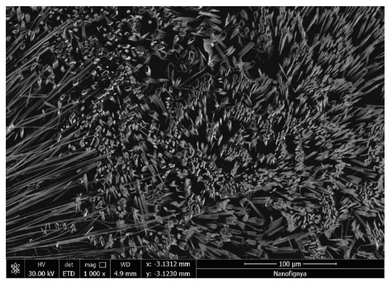

Boride fibers (high magnification)

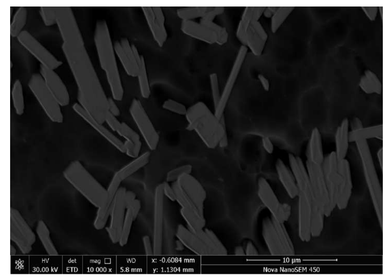

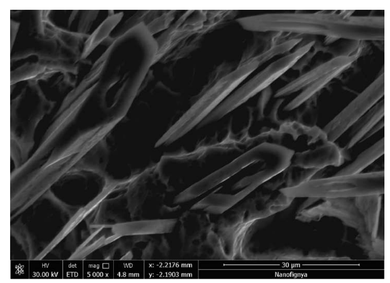

Mechanical properties

Compression at room temperature

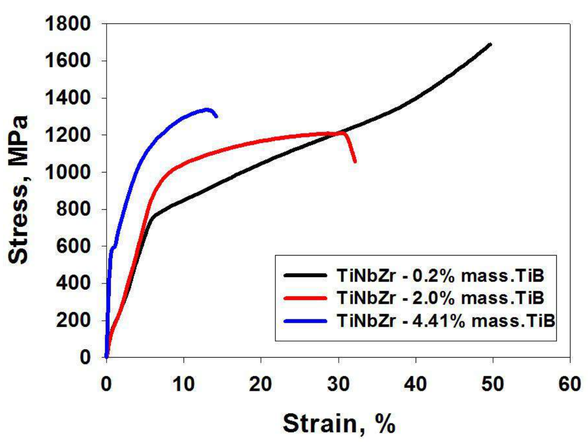

Composites	Yield strength, MPa	δ,%	Microhardness, HV
TiNbZr – 0.2 % mass. TiB	740	> 50	235±7
TiNbZr – 2 % mass. TiB	860	26	282±8
TiNbZr – 4.41 % mass. TiB	1010	9	310±8

Potential research development

- Determination of the contributions of various hardening mechanisms to the resulting strength of composites;
- Revealing the influence of post-deformation heat treatment on the structure and mechanical properties of composites;
- Establishing the effect of hot / warm rolling on the structure and mechanical properties of composites.

Acknowledgment.
The authors gratefully acknowledge the financial support from the Russian Science Foundation (Grant Number 19-79-30066). The authors are grateful to the personnel of the Joint Research Centre, Belgorod State University, for their assistance with the instrumental analysis.

III International Conference and School
"Synthesis, Structure, and Properties of High-Entropy Materials"
October 11-15, 2021

№ 30

E-mail: gleb.permyakov@yandex.ru

WIRE ARC ADDITIVE MANUFACTURING AS FABRICATION METHOD FOR BLANKS FROM CHROMIUM BRONZE

G L Permyakov, T V Olshanskaya, D N Trushnikov
Perm National Research Polytechnic University, Perm, Russian Federation

Results are provided for a study of the additive manufacturing of blanks from chromium bronze using gas metal arc cladding with cold metal transfer (CMT). The main regularities of the formation of the structure, as well as the influence of the main parameters of the mode on the geometric characteristics of the formed walls made of heat-resistant bronze, were investigated, and a test surfacing of a thin-walled cone was carried out according to a three-dimensional model. Surfacing was carried out using Fronius TPS 320i CMT gas metal arc welding / cladding equipment installed on an ARC MATE 100iC robotic complex, bronze welding wire with a content of 0.8% chromium, steel grade 12Cr18Ni10Ti substrate plate, 3 mm thick, shielding gas is Helium (He).

Working out surfacing modes:

To select the parameters of the mode, surfacing of single beads was carried out. In the process of working out the modes, the quality of the formation of the beads was assessed using visual and measuring control: the uniformity of the width and height of the bead, the absence of undercuts. As a result, the parameters of the surfacing mode were obtained:

Surfacing speed	***40 cm / min***
Wire feed speed	***3.7…7.5 м/мин***
Arc length correction	***-10…-8***
Dynamic coefficient	***-5…-3***

To carry out metallographic studies, a wall was deposited with a width of 1 bead and a height of 8 layers (Fig. 1). For surfacing, the previously worked out modes were used and the wire feed was adjusted after the first layer.

The macrostructure shows that a fine-grained equiaxed structure is formed in the first layers. In the second and third layers, the equiaxed structure gradually acquires a columnar structure. Gradually, as the layers are applied, the size (length) of the columnar grains increases. And further along the height, trans crystallization of the metal is observed, i.e. germination of columnar grains through the deposited layers. The boundaries of the deposited layers can be observed according to the different degree of metal etching.

The penetration of steel into bronze occurs in the first two layers. In the first layer, the steel is evenly distributed in the form of small drops (section 1). Sections 2 and 3 were shot at the boundary between the layers. Section 4 shows the structure of the last weld bead. In all cases, an almost straight, well-defined boundary between the columnar grains is visible; the dendritic structure is etched out inside the grains.

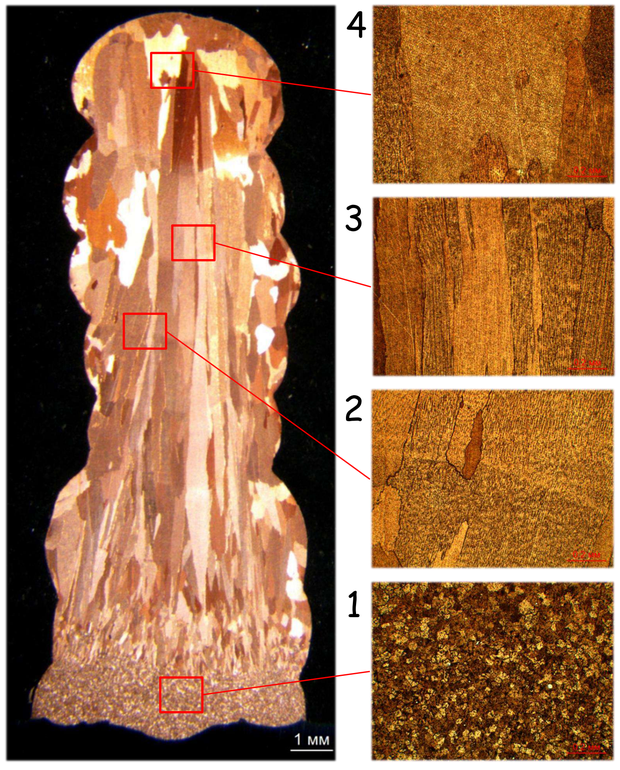

Figure 1 – Sample macrostructure (cross section) on the left and microstructure (x100) on the right

Working out surfacing of a thin-walled demonstrator:

Also, surfacing was performed on a conical specimen demonstrator with a thin wall (diameter in the lower part 40 mm, diameter in the upper part 120 mm, height 65 mm). The average height of the layers was 2 mm, the minimum wall thickness was 3.0 mm. Cladding time 45 min.

Figure 2 – Appearance of a conical thin-walled demonstrator

Conclusions:

The use of CMT cladding makes it possible to implement a process with less spreading of metal and is suitable for growing small-sized workpieces of a given shape (the wall thickness of heat-resistant bronze was from 3 to 7 mm). Metallographic studies have shown that the technology of multilayer CMT cladding ensures high-quality metal formation with an almost complete absence of pores and discontinuities (there are single pores no more than 50 μm in size), the structure acquires a columnar structure, and transcrystallization of the metal is observed, i.e. germination of columnar grains through the deposited layers. To reduce this effect and to ensure a fine-grained equiaxed structure, methods based on the introduction of ultrasonic vibration effects into the melt and on the layer-by-layer deformation effect on the deposited metal will be tested in the near future.

Acknowledgments

Present study was supported by the Ministry of Science and Higher Education of the Russian Federation at the base part of the state assignment FSNM-2020-0028, as well as by the Government of Perm Krai research project Nr. S-26/511 of March 09, 2021 and the grant from the Russian Foundation for Basic Research RFBR Nr. 20-48-596006.

III International Conference and School
"Synthesis, Structure, and Properties of High-Entropy Materials"
October 11-15, 2021

№33

vesidor@mail.ru

GLASS-FORMING ABILITY AND MAGNETIC SUSCEPTIBILITY OF Co-Fe-Si-B-Nb AMORPHOUS ALLOYS

Rusanov B.A.[1], Sidorov V.E.[1], Mikhailov V.A.[1], Svec P.Sr.[2], Janickovic D.[2]

[1]Ural State Pedagogical University, Ekaterinburg, Russia

[2]Institute of Physics Slovak Academy of Sciences, Bratislava, Slovakia

Co- and Fe-based bulk metallic glasses (BMG) and amorphous ribbons are being actively studied due to their unique magnetic and e lectrical properties. Nowadays these alloys are used as highly sensitive sensors. Unfortunately, these alloys have a low glass-forming ability (GFA). In this work we investigated crystallization processes, GFA and magnetic susceptibility of Co-Fe-Si-B-Nb-R (R = Nd, Sm, Tb, Yb) alloys in amorphous and liquid states.

Base composition $Co_{48}Fe_{25}Si4B_{19}Nb_4$ and alloys with small additions of rare-earth metals – Nd, Sm, Yb, Yb (1 at. % and 2 at. %) were prepared by remelting of pure initial components in induction furnace at 1900 K during half of hour in argon atmosphere. Amorphous ribbons (3-5 mm width and 37-40 μm thickness) were produced by planar flow casting method. BMG cylinders (2 mm in diameter and 25 mm height) were prepared by suction casting method. Amorphous structure of the alloys was checked by X-rays (Bruker D8 Advance Cu-Kα). Magnetic susceptibility of the alloys in solid and liquid states was measured by Faraday's method on an automated experimental set -up in helium atmosphere.

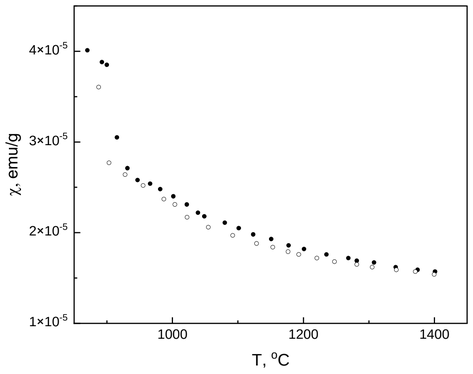

Temperature dependence of magnetic susceptibility of $Co_{48}Fe_{25}Si_4B_{19}Nb_4$ (● – heating, ○ – cooling)

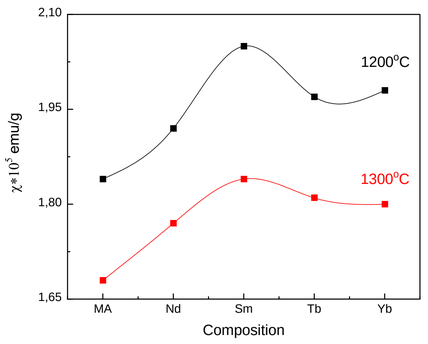

Magnetic susceptibility of $(Co_{48}Fe_{25}Si_4B_{19}Nb_4)_{98}R_2$ alloys in liquid state

Magnetic susceptibility of $Co_{48}Fe_{25}Si_4B_{19}Nb_4$ + R alloys

Alloy	$\chi_0 \cdot 10^6$, emu/g	$N(E_f)$, eV^{-1}	θ, K	$C \cdot 10^3$, emu·K/g	μ_{eff}, μ_B
$Co_{48}Fe_{25}Si_4B_{19}Nb_4$ - MA	7.1	2.7	740	7.7	2.0
MA + 1 at.% Nd	7.2	2.8	780	7.5	2.0
MA + 2 at.% Nd	7.3	2.8	800	7.8	2.0
MA + 1 at.% Sm	7.7	3.0	800	8.1	2.1
MA + 2 at.% Sm	7.9	3.1	840	8.1	2.1
MA + 1 at.% Tb	7.7	3.0	760	7.9	2.0
MA + 2 at.% Tb	8.4	3.2	770	8.0	2.1
MA + 1 at.% Yb	8.6	3.3	760	7.4	2.0
MA + 2 at.% Yb	8.4	3.2	780	7.6	2.0

Some GFA criteria of $Co_{48}Fe_{25}Si_4B_{19}Nb_4$ + R alloys

Alloy	ΔT_L, K	α	ω_J	θ, K
$Co_{48}Fe_{25}Si_4B_{19}Nb_4$ - MA	589	0.58	6.52	740
MA + 1 ат.% Nd	557	0.60	6.68	780
MA + 2 ат.% Nd	551	0.61	6.76	800
MA + 1 ат.% Sm	561	0.60	6.64	800
MA + 2 ат.% Sm	556	0.60	6.68	840
MA + 1 ат.% Tb	560	0.60	6.64	760
MA + 2 ат.% Tb	547	0.61	6.74	770
MA + 1 ат.% Yb	571	0.59	6.60	760
MA + 2 ат.% Yb	555	0.60	6.68	780

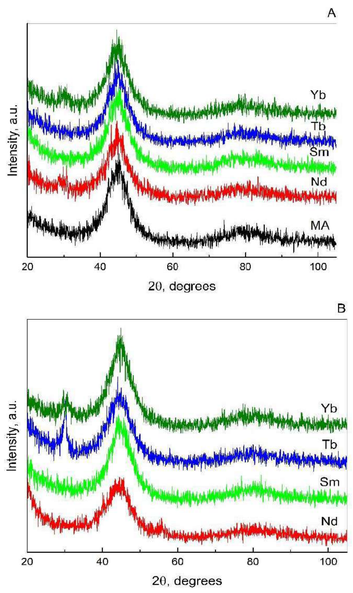

X-ray diffraction patterns of $Co_{48}Fe_{25}Si_4B_{19}Nb_4$ + R alloys. A – 1 at.% R, B – 2at.% R

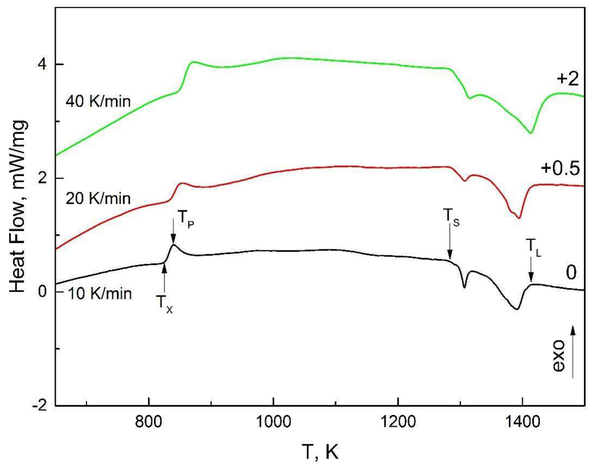

DTA thermograms of $Co_{48}Fe_{25}Si_4B_{19}Nb_4$ alloy

It was found that crystallization of these alloys goes in two stages and depends on rare-earth addition and its content in the alloy. GFA criteria were calculated. It was shown that the paramagnetic Curie temperature of the alloys in liquid state can be used as an a-priori criterion of their GFA.

The most effective additions for increasing GFA of the base composition are 2 at. % of neodymium or samarium.

TIKSAR@YA.RU

IMPROVING THE PHYSICAL AND MECHANICAL PROPERTIES OF THE FOIL FOR HIGH-VOLTAGE ELECTROLYTIC ANODES CAPACITORS BY INTRODUCING AN INTERMEDIATE ANNEALING AND MICROALLOYING WITH SCANDIUM.

Sarkisov T.S. Akopyan T.K. Sarkisov S.S.

NUST MISIS, Moscow, Russia

Oxide capacitor anodes are made of high purity aluminum (99.99 and 99.98%). The range of foil thicknesses is 0.05–0.1 mm. The criterion for its quality is the specific electrical capacity, determined for etched and oxidized (molded) foil. The amount of electrolytic capacity depends on the chemical composition, structure and texture of the foil. Foil made of high purity aluminum has relatively low strength characteristics in comparison with foil made of aluminum of lower purity (99.7% or less).

The presence of a set of necessary mechanical and structural properties, as well as the level of physical properties (in this case, electrical capacity) is a mandatory requirement for this type of foil. This complex of properties is of particular importance for high-voltage capacitor foil. Here it is necessary to take into account the fact that high-voltage foil is supplied to capacitor plants in a soft, annealed state. During recrystallization annealing, the strength characteristics decrease even more, and the correct choice of annealing modes (intermediate and final) is one of the directions for obtaining the required set of physical and mechanical properties [1, 2].

In [3], studies were made of the effect of the final recrystallization annealing modes (temperature, heating rate and isothermal holding time) on the consumer properties (specific capacity and mechanical properties) of aluminum foil for anodes of electrolytic capacitors. The studies were carried out on samples of A99 aluminum foil obtained by cold rolling from a hot-rolled strip without intermediate annealing, which amounted to a total cold deformation of 98.75%. The influence of annealing modes on the structure, texture, specific capacity and temporary resistance was revealed [3].

The averaged results of studies [3,4] of samples with only final annealing are presented in the last column of Table. 1.

Table 1. Consolidated research results

Indicator	Annealing temperature, ° C			
	Intermediate	Final		
	380	420	550	400-450
				Average research results according to [3], Best parameters
1	2	3	4	5
Specific capacity, μF / dm²	-	29	32	26
Ultimate resistance, MPa	42,0	39,2	34,6	32,0
Relative extension,%	5,6	4,1	3,7	3,6
Average grain size, μm	78	72	80	105
Reflection intensity ratio le/lm, {200}, not less than %	-	90	95	90

Figure 1 shows the effect of the reflection n intensity of the {200} cubic texture on the specific capacitance of a high-voltage foil.

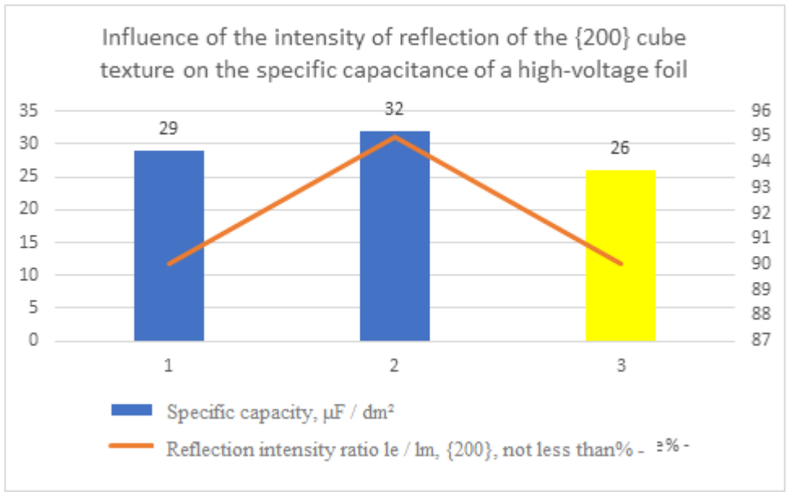

Figure 1. Influence of the intensity of reflection of the {200} cube texture on the specific capacitance of the high-voltage foil.

In [4], it was found that there is a complex dependence of the maximum specific capacity of the foil for high-voltage anodes on the average grain size and their crystallographic orientation, in this case, the maximum value of the cubic texture, at admissible values of the temporary resistance of the foil. And also with an increase in the intensity of the cubic texture from 90% to 95%, the specific capacity increases from 29 to 32 μF / dm2, in the case of using intermediate annealing at a temperature of 380 ° C and further final annealing at temperatures of 420 ° C and 550 ° C, respectively.

We also evaluated the comparison of the introduction of intermediate annealing on samples microalloyed with scandium (Al + 0.05% Sc, Al + 0.1% Sc, Al + 0.3% Sc), where the dynamics of a similar result was obtained, but with lower capacitance values. This shows the greater efficiency of the use of thermal deformation modes to increase the capacity on foils without microalloying in comparison with microalloying on this type of product.

1. Novikov I. I., Zolotorevsky V.S., Portnoy V.K., Belov N. A., Livanov D.V. et al. Metallurgy. V1. Fundamentals of metal management. - M.: Publishing house MISIS, 2014 .-- 496 p.

2. Luts A.R., Suslina A.A. Aluminum and its alloys: textbook. - Samara: Samara State Technical University, 2013 .-- 81 p.

3. Sarkisov S.S. Study of the influence of final annealing modes on consumer properties of aluminum foil for anodes of high voltage electrolytic capacitors. Tsvetnye Metally. 2019. No. 3. P. 58–63. DOI: 10.17580 / tsm. 2019.03.08.

4. Sarkisov T.S., Belov N.A, Sarkisov S.S., Dolbachev A.P. Improving the physical and mechanical properties of the foil for high-voltage electrolytic anodes capacitors by introducing an intermediate annealing Tsvetnye Metally. 2021. No. 5. P. 65-70. DOI: 10.17580 / tsm. 2021.05.08

III International Conference and School
"Synthesis, Structure, and Properties of High-Entropy Materials"
October 11-15, 2021

№ 35

High Temperature Oxidation Resistance of Refractory High Entropy Alloys

ostovarim@susu.ru

Ostovari Moghaddam A., Veselkov S. N. , Shaburova N. A. , Sudarikov M. V., Samoilova O. V , Pratskova S. E. , Trofimov E. A.

South Ural State University, Chelyabinsk, Russian Federation

1- Introduction

High entropy alloys (HEAs) are defined as alloying system consisted of five or more principal elements with typically equiatomic or near equiatomic ratio, which occasionally exhibit extraordinary properties [1]. Among different types of HEAs, refractory HEAs (RHEAs) are considered as the most promising alloy systems to design new materials for high temperature applications beyond Ni based superalloys [2]. Besides, W-containing HEAs are potential candidate for high temperature applications such as plasma facing material in nuclear reactors owing to high melting temperature, high thermal conductivity and small tritium retention of tungsten. However, a systematic study on the oxidation resistance of W-containing HEAs is still lacking.

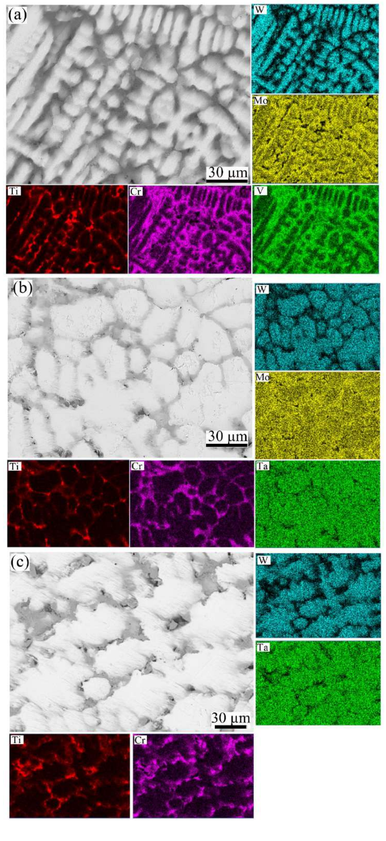

Fig. 1 BSE-SEM micrograps and the corresponding EDS elemental maps of the constiruent elements for (a) WMoTiCrV, (b) WMoTaTiCr, (c) WTaTiCr HEAs.

1- Experimental

Equimolar WTaTiCr, WMoTaTiCr, and WMoVTiCr alloys were fabricated by arc-melting process under argon atmosphere using high purity (> 99.9 wt. %) metal powders. Pure powders were first weighted and thoroughly mixed in an agate mortar. The mixed powders were then loaded into a water-cooled copper mold and arc melted under Ar atmosphere. The bottoms were flipped over and remelted five times to ensure chemical homogeneity. The fabricated bottoms were then cut and polished for structural analysis. X-ray diffraction (XRD) was performed on a Rigaku Ultima IV X-ray diffractometer. Microstructural analysis was studied on a scanning electron microscope (SEM) Jeol JSM7001F equipped with energy-dispersive X-ray spectroscopy detector (EDS; Oxford INCA X-max 80). Quantitative oxidation resistance of the samples were measured using a Q-1500D derivatograph (Paulik and Erdei, Hungary) under isothermal conditions at 1000 ºC for 10 h in air atmosphere. To reveal the oxidation behavior of the materials, the oxidized surfaces were then thoroughly analyzed by XRD and SEM-EDS analysis.

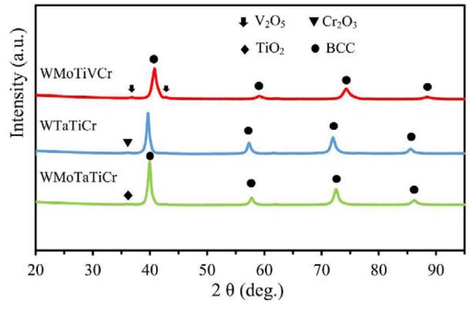

Fig. 2 XRD patterns of the as-cast RHEAs

1- Results and discussion

In this study, we investigated the oxidation resistance of several W-containing refractory HEAs at high temperatures to further examine the formation of complex oxides layer on the surface of these alloys. The equimolar WMoTiVCr, WMoTaTiCr, and WTiTaCr alloys were fabricated by arc-melting process under argon atmosphere using high purity (> 99.9 wt. %) metal powders. The as cast alloys exhibited dendritic microstructure and elemental segregation. Typically for all the alloys W and Ta segregated in the dendritic arms and Ti, Cr, Mo, and V segregated into the inter-dendritic regions (Figure 1). However, in spite of these segregations, a nearly single BCC solid solution phase (Figure 2) was observed for all the samples. Oxidation behavior of the samples were studied at 1000 °C for 10 h in air atmosphere. WMoTiVCr alloy exhibited very low resistance against high temperature oxidation mainly due to the formation of a highly porous TiO2 rich scale layer. By substituting V with Ta in WMoTaTiCr, a WO3 and CrTaO4 rich oxide layer was dominated and the oxidation resistance was improved (Figure 3). A similar oxide layer was also formed on the surface WTiTaCr alloy.

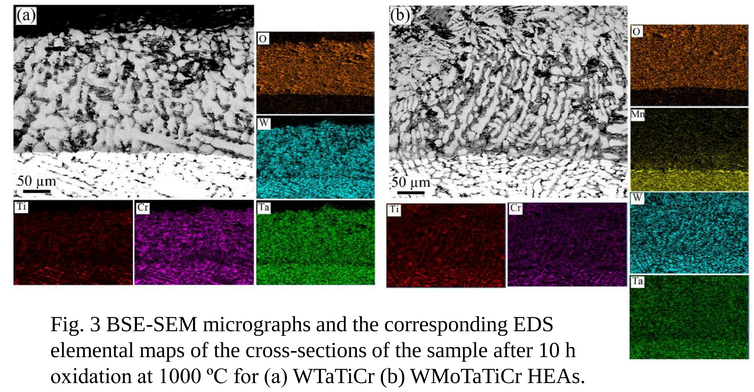

Fig. 3 BSE-SEM micrographs and the corresponding EDS elemental maps of the cross-sections of the sample after 10 h oxidation at 1000 ºC for (a) WTaTiCr (b) WMoTaTiCr HEAs.

References

1. George E.P., Curtin W.A., Tasan C.C. High entropy alloys: A focused review of mechanical properties and deformation mechanisms. Acta Materialia. 2020 Apr 15;188:435-74.

2. Moghaddam A.O., Cabot A., Trofimov E.A. Does the pathway for development of next generation nuclear materials straightly go through high-entropy materials? International Journal of Refractory Metals and Hard Materials. 2021 Feb 20:105504.as

The research was funded by RFBR and Chelyabinsk Region, project number 20-43-740018.

III International Conference and School
"Synthesis, Structure, and Properties of High-Entropy Materials"
October 11-15, 2021

№36

pilipenko.arina25@mail.ru

MICROSTRUCTURE, MECHANICAL AND ELECTRICAL PROPERTIES OF COPPER ALLOY AFTER COLD PLASTIC DEFORMATION

Pilipenko A.G.[1], Bodyakova A.I.[1,2]

[1]Belgorod State University, Belgorod, Russia

[2]National University of Science & Technology (MISIS), Moscow, Russia

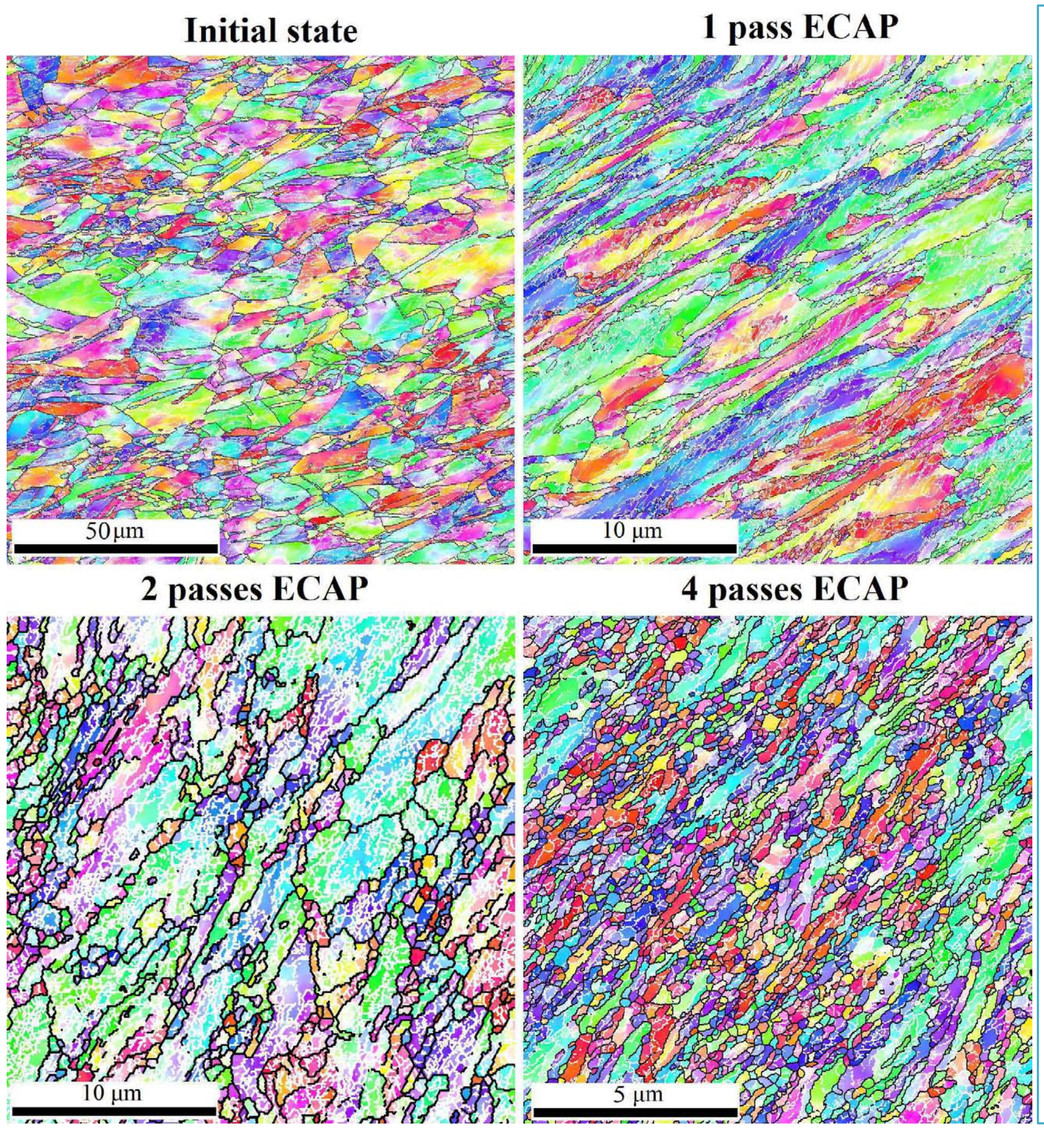

Experiment

The object of the present study was copper alloy a Cu-0.25%Mg (wt.%). The ingots were forged at 800 °C and rolled at 450 °C. The average grain size in the initial state was about 2.0 μm, dislocation density – 4.2×10^{14} m^{-2}. The yield strength (YS) and the ultimate tensile strength (UTS) achieved of about 375 and 425 MPa, respectively. Elongation was about 23%, electrical conductivity – 81% IACS. Then, the samples were subjected to 1, 2 and 4 passes of equal channel angular pressing (ECAP) via route Bc with an intersection angle of the matrix channels of 90 ° at room temperature. The microstructure was studied by Nova NanoSEM 450 scanning electron microscope equipped with an electron backscattered diffraction analyzer. The samples were electro-polished in electrolyte with 25%HNO_3 and 75%CH_3OH at -20 °C and voltage of 10 V using a Tenupol 5 equipment. The microstructure parameters were calculated using OIM Analysis software. The mechanical properties were investigated using an Instron 5882 machine with an initial strain rate of 2×10^{-3} c^{-1}. The electrical conductivity was estimated by the eddy current method on the Constant K-6 equipment.

Results

1. The 1st pass of ECAP led to the formation of the high density of low-angle boundaries (LAB) and a decrease in the average grain size to 0.9 μm.
2. Increase of the ECAP passes number was accompanied by the transformation of LAB to high-angle boundaries (HAB).
3. The ultrafine-grained structure with an average grain size of about 0.6 μm and the dislocation density of 9.8×10^{14} m^{-2} was developed after 4 passes of ECAP.
4. The YS and UTS after 4 ECAP passes were 540 MPa and 560 MPa, respectively.
5. The 4th ECAP pass was accompanied by a sharp decrease in the elongation to 9.1%.
6. After 4 ECAP passes the electrical conductivity decreased to 77.2 %IACS.

The financial support received from the Ministry of Science and Higher Education of the Russian Federation, under President grant No. 075-15-2020-407 is gratefully acknowledged. The work was carried out using the equipment of the Joint Research Center of Belgorod State National Research University «Technology and Materials».

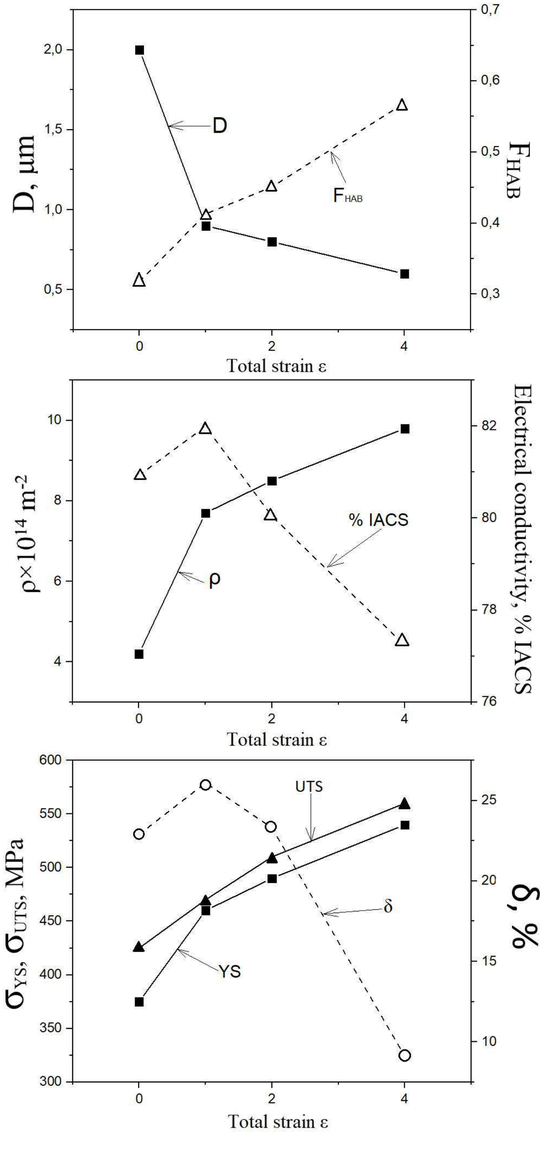

III International Conference and School
"Synthesis, Structure, and Properties of High-Entropy Materials"
October 11-15, 2021

№ 38

viktor.semin.tsk@gmail.com

CRYSTALLIZATION OF Ti-Ni-Ta METALLIC GLASS SURFACE ALLOY FABRICATED ON TINI SMA SUBSTRATE BY ADDITIVE THIN-FILM ELECTRON-BEAM SYNTHESIS

Semin V. O.
Institute of Strength Physics and Materials Science SB RAS, Tomsk, Russia

Motivation. *TiNi shape memory alloys (SMAs) are promising metallic biomaterials due to combination of superelastisity and high corrosion resistance. However, there are serious limitations of implementation of TiNi SMAs in biomedicine arising from a risk of toxic Ni release into the adjacent tissues, as well as insufficient level of X-ray visibility. These limitations can be overcome by fabrication of a Ti-Ni-Ta metallic glass surface alloy (MGSA) on the TiNi substrate. The approach of surface alloy synthesis is realized through the multiple (10 cycles) alternation of magnetron co-deposition of Ti60Ta40 (at. %) thin (100 nm) film and their liquid-phase mixing with the TiNi substrate by low-energy high current electron beam (≤ 15 keV, ~2 J/cm2).*

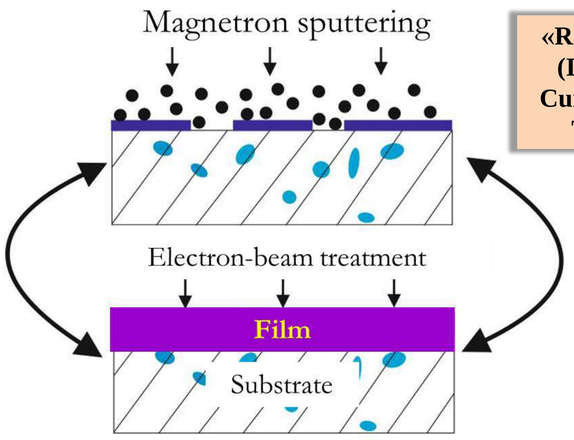

«RITM-CP» facility (Institute of High Current Electronics, Tomsk. Russia)

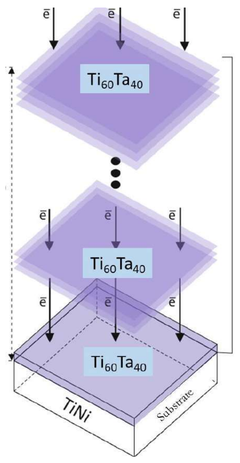

Methods. *The structure of samples was studied by high resolution transmission electron microscopy (HRTEM) on JEM 2100F operated at 200 kV and in-situ X-ray diffraction technique on Shimadzu 7000S in copper radiation. Cross-sectional TEM studies were carried out using the bright and dark field regimes in the combination with a selected area electron diffraction and nano-beam diffraction. The foils were prepared by mechanical grinding and ion milling using EM 09100IS (JEOL, Japan). In order to extract the radial distribution function, a series of NBD patterns were collected with a probe-beam diameter of 2 nm. Annealing of MGSA was carried out in vacuum (P = 10^{-5}–10^{-6} mbar) at T = 673 K for 10 min.*

Radial distribution function (RDF)

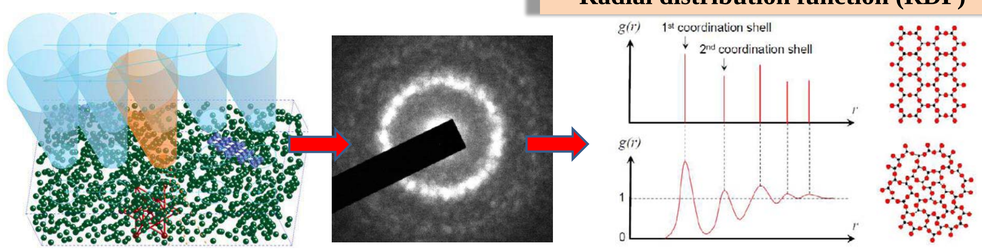

Results. *It has been found that as-cast MGSA shows completely amorphous structure (~ 2 μm thickness) with gradient chemical composition and, relative to conventional metallic glasses, appears nonhomogeneous in structure depending on various atomic arrangements in the first and second neighboring shells (Fig. 1).*

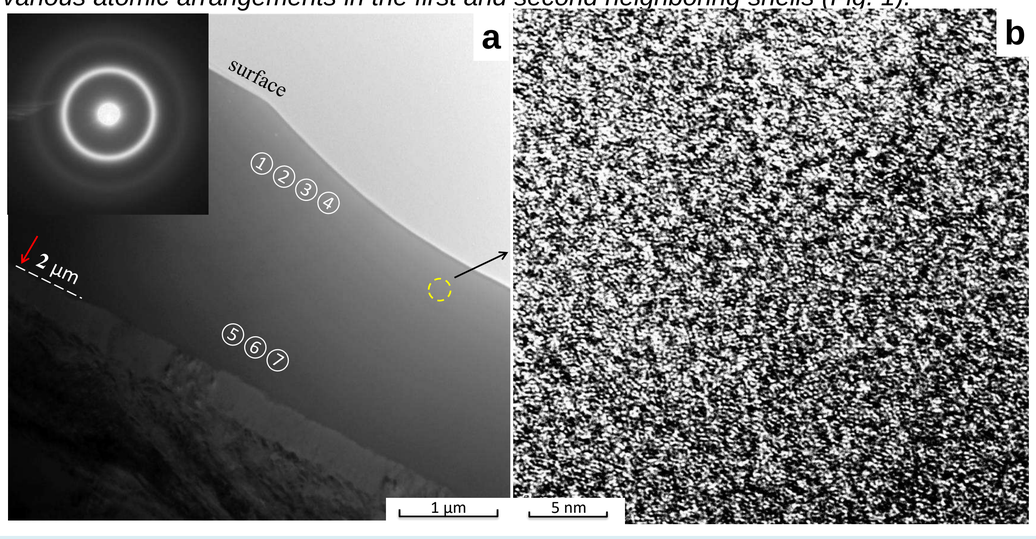

Fig.1. Bright-field (a) and HRTEM images of the as-cast Ti-Ni-Ta MGSA. Nano-beam diffractions (marked by numerals) were utilized to resolve RDFs (c, d). The experimentally obtained PDFs are oscillating functions with several well-defined maxima in the range of 2 Å-10 Å originating from structural correlations in the medium-range scale.

In-situ XRD study revealed that crystallization of amorphous matrix started at 773 K (Fig. 2a). However, nanodevitrification occurred at lower annealing temperatures (673 K) and accompanied by formation of icosahedral quasicrystals (Fig. 2b,c).

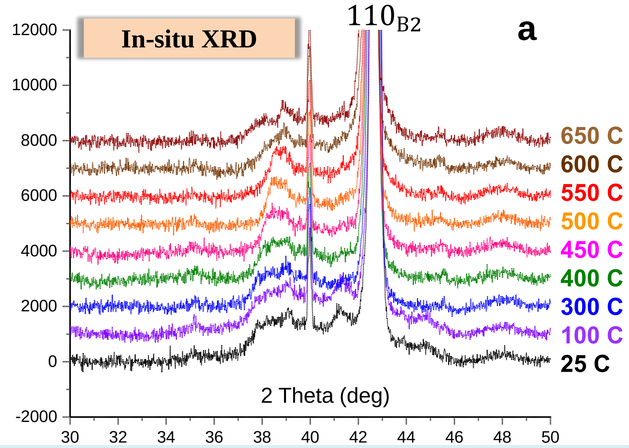

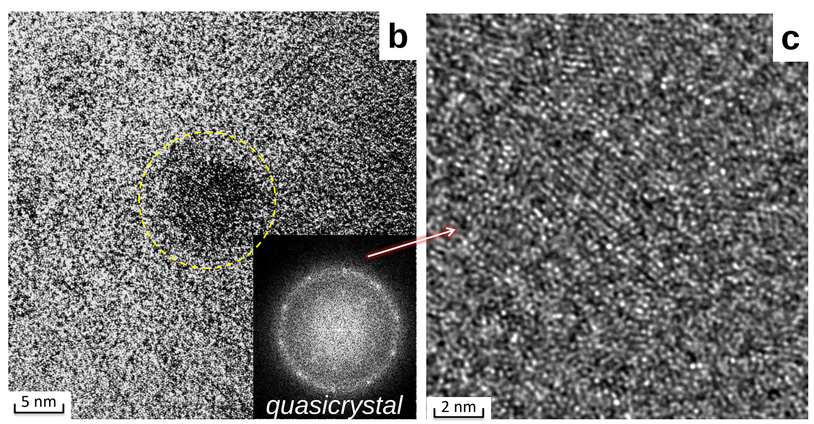

Fig.2. Fragments of XRD patterns (a) collected at different temperatures (in–situ heating). HRTEM images (b, c) and corresponding FFT pattern show an icosahedral phase embedded into glassy matrix after annealing at 673 K (10 min).

III International Conference and School
"Synthesis, Structure, and Properties of High-Entropy Materials"
October 11-15, 2021

№ 40

THERMODYNAMICS OF VAPORIZATION PROCESSES IN THE GeO_2–ZnO SYSTEM

E-mail: prostreet02@rambler.ru

Smirnov A.S., Smorchkov K.G., Gribchenkova N.A., Alikhanyan A.S.

Kurnakov institute of general and inorganic chemistry of the Russian Academy of Sciences, Moscow, Russia

The study of the GeO_2–ZnO system was performed by the Knudsen effusion mass spectrometry in the temperature range 1140–1280 K. The Ge^+, GeO^+, Zn^+, and O^+ ions were registered in the mass spectrum of the gas phase over the heterogeneous samples [GeO_2 + Zn_2GeO_4], [Zn_2GeO_4 + ZnO] and compound Zn_2GeO_4 at 1260 K.

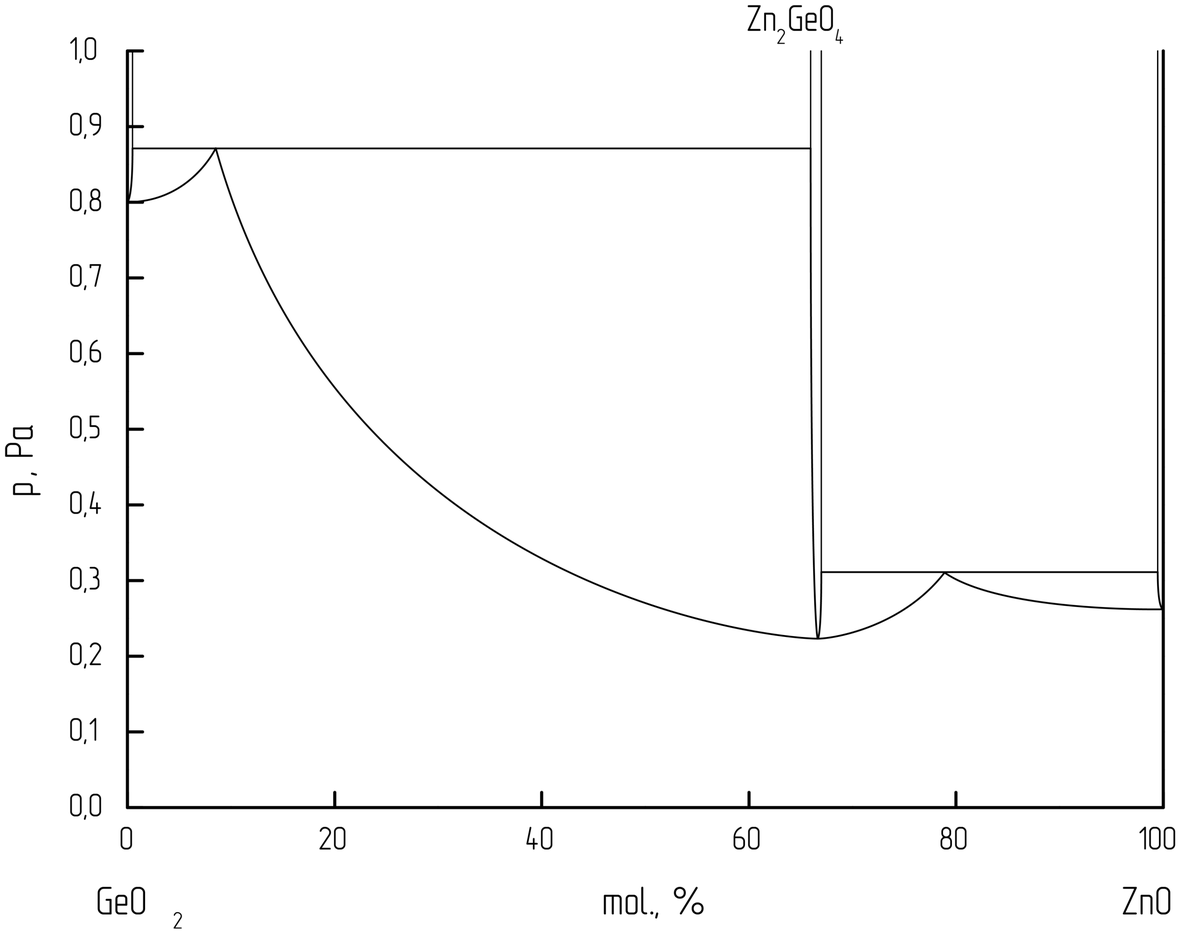

Figure 1. A *p*–*x*-section of the quasi-binary system GeO_2–ZnO at 1260 K.

Table 1. Partial pressure of the vapor species and the total vapor pressure over the quasi-binary system GeO_2–ZnO at 1260 K

Phase composition	Partial pressure of vapor species, Pa			Total vapor pressure, Pa
	p(GeO)	*p*(O_2)	*p*(Zn)	
GeO_2	0.533	0.267	-	0.800
GeO_2 + Zn_2GeO_4	0.611	0.203	0.057	0.871
Zn_2GeO_4	0.058	0.056	0.109	0.223
Zn_2GeO_4 + ZnO	0.049	0.079	0.183	0.311
ZnO	-	0.087	0.174	0.262

Determination of the qualitative and quantitative composition of the gas phase made it possible to calculate the activities of the components in heterogeneous regions: $a(GeO_2)=0.05$, $a(ZnO)=0.5$. Using the found activities of the components, the Gibbs free energy of the reaction was calculated:

$$Zn_2GeO_4 = ZnO+GeO_2$$

The enthalpy of formation of the compound Zn_2GeO_4 was −1303.9±43.1 kJ/mol.

In addition, the experimentally found values of the total pressure over different phase fields were used to construct the principal *p*-*x*-section of the quasi-binary system GeO_2–ZnO.

This work is supported by the Russian Science Foundation under grant 21-13-00086.

III International Conference and School
"Synthesis, Structure, and Properties of High-Entropy Materials"
October 11-15, 2021

№41

Wangjiankun_s@163.com

温州大學 WENZHOU UNIVERSITY

Research on the microstructure and strengthening mechanism of CoCrFeNiSix (x=0, 0.25, 0.5, 0.75) based on arc additive manufacturing

Wenzhou University

file name: ***Jiankun Wang*** *professor: Xizhang Chen*

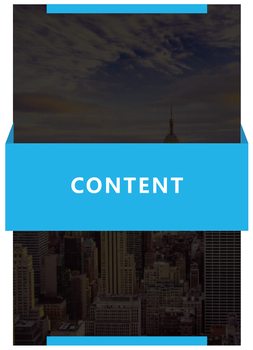

Introduction

In 2004, Taiwanese scholars proposed the concept of multi-principal high-entropy alloys. Each element has a high atomic ratio, but a single element does not exceed 35%, breaking the traditional framework. This discovery opened the door to research on high-entropy alloys. However, in the field of high-entropy alloys, there is little research on the effect of non-metallic materials on high-entropy alloys.

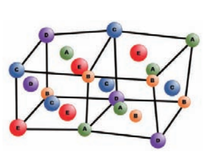

Schematic diagram of multi-component solid solution

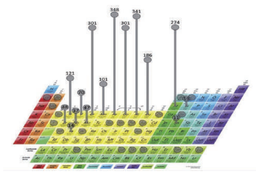

Introduction

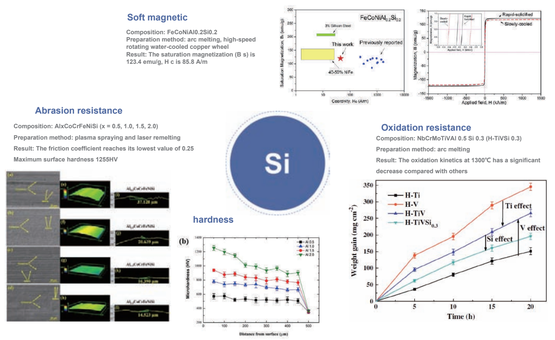

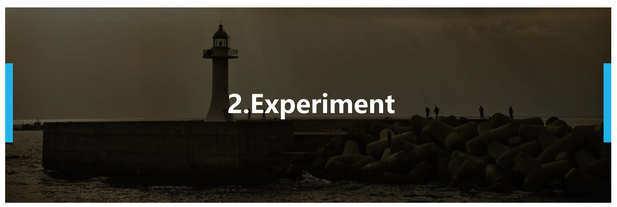

Experiment

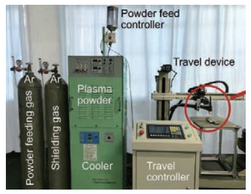

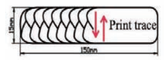

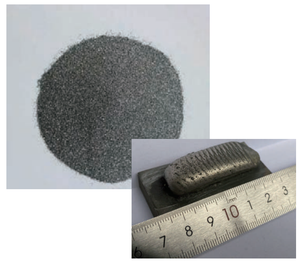

High temperature, high processing efficiency, high utilization rate of metal powder

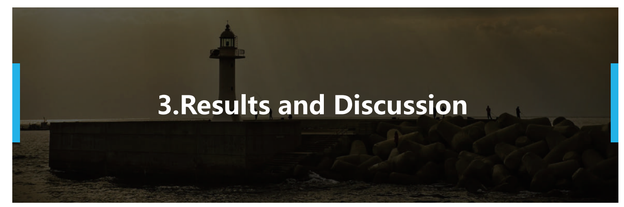

Experimental results

Stretching result

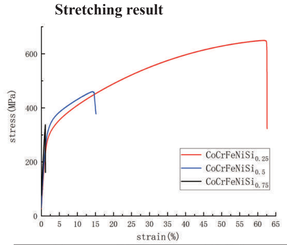

hardness

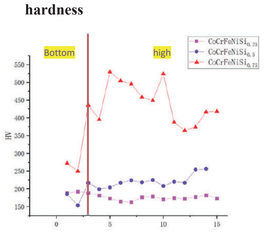

成分	屈服强度(Mpa)	断裂强度(Mpa)	延伸率(%)
CoCrFeNi	187.86±7.98	-	-
$CoCrFeNiSi_{0.25}$	285.62±10.26	629.54±24.46	56.01±7.43
$CoCrFeNiSi_{0.5}$	304.70±11.53	451.94±41.82	13.77±7.42
$CoCrFeNiSi_{0.75}$	354.26±71.64	354.26±71.64	1.30±0.21

During additive manufacturing, the Si element at the bottom will splash due to melt droplets, resulting in different structures and different material properties.

Experimental results

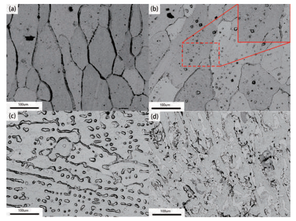

Metallographic structure diagram of different Si content: (a)CoCrFeNi， (b)CoCrFeNiSi0.25，(c)CoCrFeNiSi0.5，(d)CoCrFeNiSi0.75

The precipitation phase gradually increased. In Figure c, it is obvious that a part of $Cr_3Ni_5Si_2$ precipitates at the grain boundary, which leads to a decrease in elongation.

XRD result

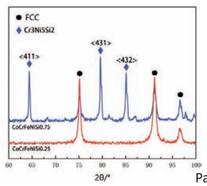

SEM

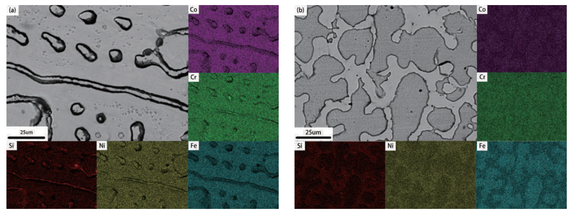

SEM&EDS Energy spectrum analysis result (a) $CoCrFeNiSi_{0.5}$,(b)$CoCrFeNiSi_{0.75}$

It can be seen from the results that Co and Fe are obviously dim in the intermetallic compound, indicating that these two elements are mainly concentrated in the FCC phase. The content of Si element itself is small, so even if there is more in the intermetallic compound, the color difference is not obvious.

EDS

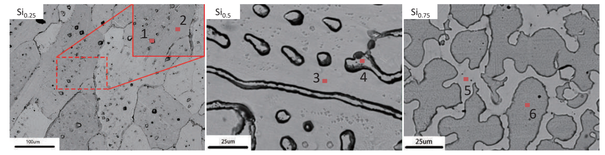

	Co(wt%)	Cr(wt%)	Fe(wt%)	Ni(wt%)	Si(wt%)
1	27.06	25.12	23.54	23.81	0.48
2	26.59	20.48	24.39	27.02	1.52
3	27.11	19.96	26.16	25.17	1.59
4	23.00	22.75	18.88	31.03	4.34
5	25.30	19.94	21.65	29.39	3.72
6	27.05	20.01	25.91	24.71	2.31

It can be seen from the EDS results that there are more Si elements in $Cr_3Ni_5Si_2$. But in $CoCrFeNiSi_{0.25}$, the crystallized matter fell off, so the result is just the opposite.

analyze

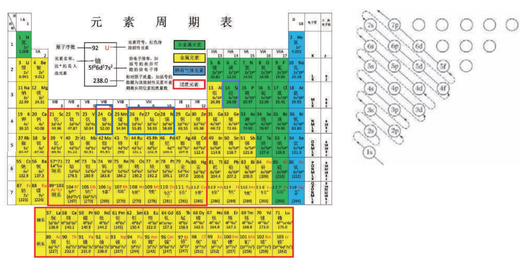

The internal bonding of intermetallic compounds is complex and difficult to figure out. Ordinary metal bonds are easier to bond together.

Yuan, L. 和H.M. Wang. 《Corrosion Behaviors of a γ-Toughened Cr13NiSiSi2/Cr3NiSSi2 Multi-Phase Ternary Metal Silicide Alloy in NaCl Solution》. *Electrochimica Acta* 54, 2 (2008.12): 421–29. https://doi.org/10.1016/j.electacta.2008.07.056

EBSD analyze

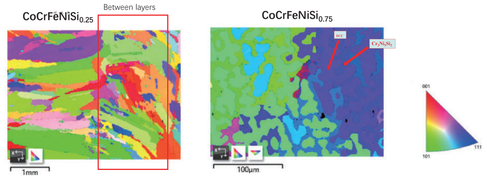

The grain size of $CoCrFeNiSi_{0.25}$ is larger and slender, and the interlayer structure is relatively fine.

The orientation of $Cr_3Ni_5Si_2$ is different in the two adjacent grains

The driving force for segregation is the internal energy difference: suppose the internal energy of an atom in the grain and the grain boundary are respectively E_i and E_g

$$\Delta E_a = E_i - E_g$$

The increase of Si element causes $Cr_3Ni_5Si_2$ to be generated from inside the initial grains and grow up. Then, in order to maintain the energy balance of the system, some intermetallic compounds gather at the grain boundaries.

Conclusion

1. In the high-entropy alloy produced by arc additive manufacturing, Si element is easy to form intermetallic compounds with Cr and Ni, and then dispersed between the grains; with the increase of Si element, $Cr_3Ni_5Si_2$ is produced and increased, and then partly to the grain boundary Gather to maintain the balance of the entire system;

2. The intermetallic compound $Cr_3Ni_5Si_2$ has high hardness, which can greatly increase the hardness of CoCrFeNi alloy, from the original 175Mpa to more than 400Mpa;

3. The intermetallic compound $Cr_3Ni_5Si_2$ can increase the yield strength of the material, but the elongation of the material will be reduced a lot, so the appropriate Si element content can effectively improve the performance of the material.

III International Conference and School" Synthesis, Structure, and Properties of High-Entropy Materials" October 11-15, 2021

THERMODYNAMICS OF COMPLEX COMPOUNDS BASED ON ZnO and Nb_2O_5

Smorchkov K.G., Smirnov A.S., Gribchenkova N.A., Alikhanyan A.S.
Kurnakov Institute of General and Inorganic Chemistry of the Russian Academy of Sciences

Ceramics based on zinc niobates are promising materials in microwave electronics due to its electromagnetic parameters. To obtain functional materials with specified physical and physicochemical properties, knowledge of their thermodynamic characteristics, as well as the thermodynamics of vaporization processes, is required. In this regard, we carried out high-temperature study of the vaporization processes and thermodynamic properties of the ZnO – Nb_2O_5 system. This study was carried out by the Knudsen effusion method with mass spectral analysis of the gas phase in the temperature range 1200–1500 K. Mass spectral analysis showed that the saturated vapor over the studied system in the entire range of compositions consists mainly of zinc atoms and oxygen molecules.

Standard enthalpies of heterophase reactions $\Delta_r H^O_{298.15}$ (kJ / mol), calculated according to the 2nd and 3rd laws of thermodynamics

Reaction	2-law	3-law	Recommended value
$ZnO(cr) = Zn(g) + 0.5\ O_2$	483.7 ± 15.5	484.7 ± 7.0	484.7 ± 7.0
$Zn_3Nb_2O_8(cr) = ZnNb_2O_6(cr) + 2Zn(g) + O_2$	941.3 ± 35.7	991.5 ± 16.0	966.4 ± 25.9
$ZnNb_2O_6(cr) = Nb_2O_5(cr) + Zn(g) + 0.5O_2$	509.4 ± 13.0	529.1 ± 7.5	516.9 ± 10.0
$ZnNb_2O_6(cr) = 1/17\ Zn_2Nb_{34}O_{87}(cr) + 15/17\ Zn(g) + 15/34\ O_2$	481.6 ± 24.6	467.2 ± 7.5	474.2 ± 16.1
$Zn_2Nb_{34}O_{87}(cr) = 17\ Nb_2O_5(cr) + 2\ Zn(g) + O_2$	1061.5 ± 5.3	1077.1 ± 16.0	1068.5 ± 8.5

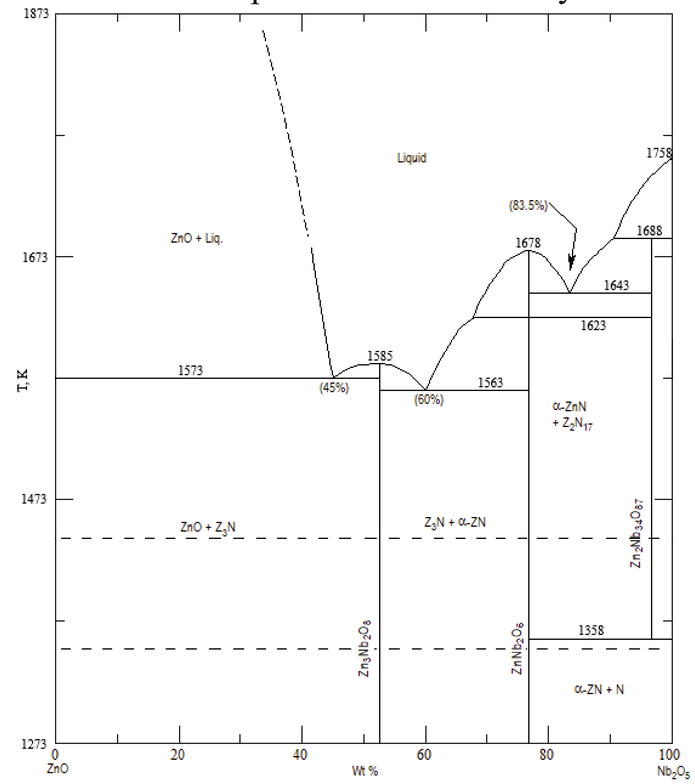

Phase diagram of the ZnO-Nb_2O_5 system [1]

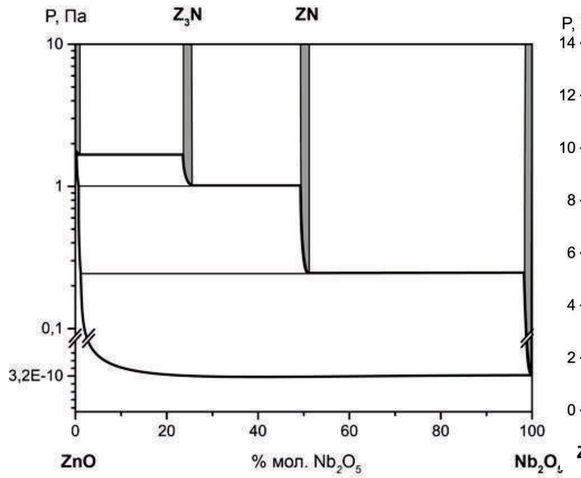

P–x section of the phase diagram at T = 1353 K

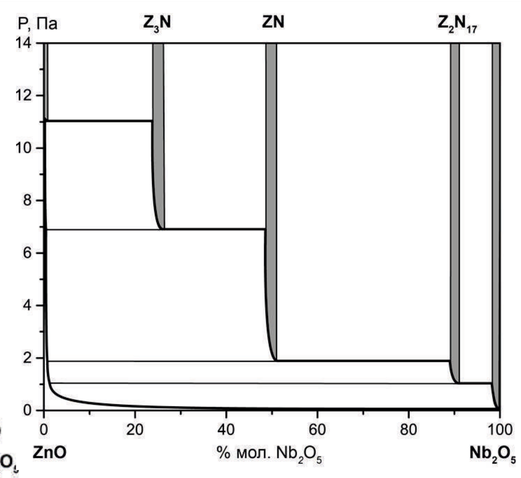

P–x section of the phase diagram at T = 1443 K

Standard enthalpies of formation of zinc niobates (kJ/mol)

Compound	$-\Delta_f H^O_{298.15}$ (from oxides)	$-\Delta_f H^O_{298.15}$	$-\Delta_f H^O_{298.15}$ (from oxides, recommended value)
$Zn_3Nb_2O_8(cr)$	50.1 ± 32.1	2992.0 ± 30.2	50.0 ± 20.0
$ZnNb_2O_6(cr)$	48.3 ± 21.3	2292.4 ± 19.9	40.5 ± 15.0
$Zn_2Nb_{34}O_{87}(cr)$	89.7 ± 19.4	33056.1 ± 15	90.9 ± 15.0

Conclusions.

The thermodynamic characteristics of the ZnO-Nb_2O_5 system found in this study can be very useful in the synthesis of dielectric ceramics with high physical characteristics.

1 Dayal, R. R. The binary system ZnO-Nb_2O_5. Journal of the Less Common Metals, 26 (3), 1972, P. 381–390

This work was supported by the Russian Science Foundation, Grant 21-13-00086.

III International Conference and School
"Synthesis, Structure, and Properties of High-Entropy Materials"
October 11-15, 2021

№ 43

Effect of tempering on fracture toughness of B-added 9%Cr martensitic steels

E. Tkcahev, Yu. Borisova
Belgorod State University, Belgorod, Russia
tkachev_e@bsu.edu.ru

E-mail
tkachev_e@bsu.edu.ru

Introduction

9%Cr martensitic steels are an important class of structural materials for elevated temperature applications because of combination of good corrosion resistance and high creep strength. Several concepts have been proposed for the development of new creep-resistant steels with increased creep resistance. Recently, considerable interest was paid to boron containing 9-10%Cr steels. A small amount of B was found useful to improve the stability of tempered martensite lath structure (TMLS) under creep conditions especially due to fine dispersion of $M_{23}(C,B)_6$ particles.
The precipitation behavior and mechanical properties of high-chromium martensitic steels are closely connected with tempering temperature. Thus, the present work describes the effect of tempering on impact toughness of two modified 9% Cr steel with high B and low N contents.

Results

The toughness of the normalized TaB-added steel is 24 J/cm^2 which is lower than that of B-added steel (43 J/cm^2). This may result from difference in prior austenite grain (PAG) size since the mean PAG size in TaB-added steel is about twice lower than that in B-added steel. Both steels are characterized by significant drop in impact toughness below 10 J/cm^2 after tempering at 500°C. Tempered martensite embrittlement of studied steels is accompanied by decrease in the maximum load P_f from 33.5 to 13.4 kN for B-added steel and from 28.8 to 6.4 kN for TaB-added steel. The increase in tempering temperature to 750°C led to change in fracture mode in B-added steel from brittle to ductile with high toughness of 244 J/cm^2. In contrast the impact toughness of TaB-added steel tempered at 750°C is only 32 J/cm^2. However, further increase in tempering temperature to 780°C leads to increase in impact energy of TaB-added steel to 135 J/cm^2. The corresponding value of impact toughness of the B-added steel after the same heat treatment is 265 J/cm^2.
Such difference in impact toughness of studied steels tempered at 780°C can be attributed to the decreased value of P_f=21.6 observed for TaB-added steel as compared to that for B-added steel P_f=27.3. Since the value of maximum load during impact test represents the ease of the initiation of the crack, it was concluded that the decreased toughness of the studied Ta-added 9% Cr steel is associated with reduced critical stress required for crack initiation.

Experimental

The studied steels Fe-0.1C-9Cr-1.8W-0.6Mo-3Co-0.05Nb-0.2V-0.012B-0.007N (%wt.) (hereafter B-added steel) and Fe-0.1C-9Cr-1.8W-0.6Mo-3Co-0.05Nb-0.2V-0.013B-0.007N-0.085Ta (hereafter TaB-added steel) are similar in chemistry except in Ta content. The B-added and TaB-added steels were normalized at 1060°C for 0.5h and 1050°C for 0.5h respectively and then tempered at 500, 750 and 780°C for 3 h. The Charpy impact tests were performed on standard V-notch specimens at room temperature using Instron IMP460 machine with a 300 J capacity.

The influence of tempering on impact toughness and length of stable crack propagation of TaB-added steel

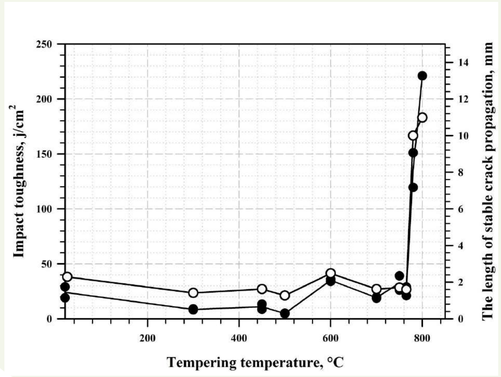

The dependence of length of stable crack propagation on maximum load during impact test of TaB-added steel

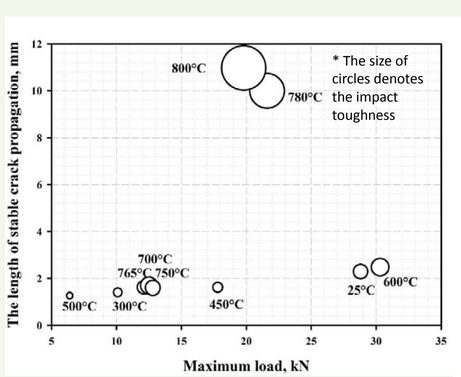

SEM Fractography

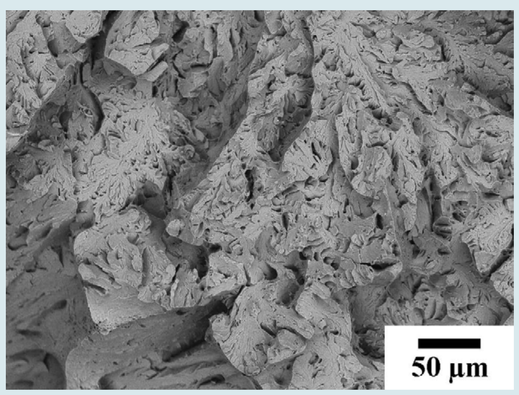

TaB-added 9%Cr steel tempered at 765°C

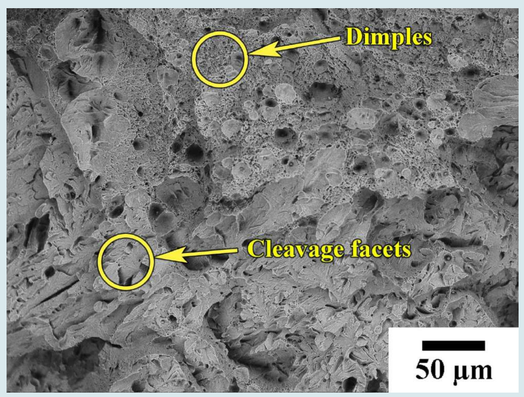

TaB-added 9%Cr steel tempered at 780°C

The load-deflection curves of studied B-added and TaB-added 9%Cr steels

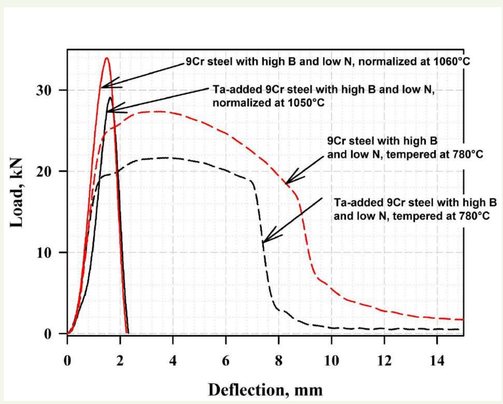

The reported study was funded by the Russian Science Foundation, under grant No. 21-79-00067.

III International Conference and School
"Synthesis, Structure, and Properties of High-Entropy Materials"
October 11-15, 2021

Degradation kinetics of two-layer tissue equivalents based on sodium alginate in fluids simulating extracellular body fluids

Fetisova V.E.
Baikov Institute of Metallurgy and Materials Science RAS, Moscow, Russia
e-mail: victoria.phetisova@yandex.ru

№44

Relevance

Every day many people face skin injuries related to diseases, burns and frostbite. Studies have shown that one of the most promising ways to treat such wounds is to replace the damaged areas directly with skin equivalents made of polymers of plant origin, such as sodium alginate. Sodium alginate has unique properties that allow it to form strong three-dimensional porous matrices of various shapes, which makes it possible to use it for skin regeneration.

For such materials to be suitable for use in wound care, they need to be double-layered. In this case, and the porous layer adjacent directly to the wound will provide rapid vascularization and absorption of excess fluid (lymph) from the wound, which will accelerate the patient's recovery; and the outer layer will maintain the temperature and protect the wound from the environmental influences. To perform these functions, the skin equivalent must be insoluble in water. For this reason, cross-linking, a method of joining individual polymer chains together that leads to insolubility of the materials, is necessary.

Materials

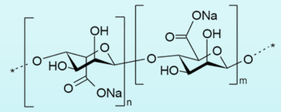

Sodium alginate

Crosslinking salts:

- $SrCl_2$
- $BaCl_2$
- $Ba(CH_3COO)_2$
- $Ca(NO_3)_2$
- $CaCl_2$

Sodium alginate cross-linking scheme

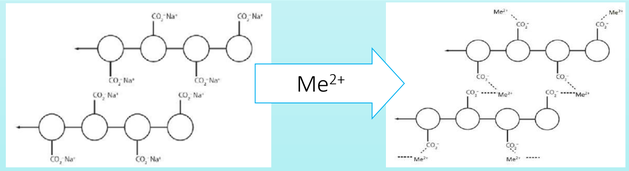

Cross-linking

Cross-linking of such materials was carried out via bivalent metal cations: sodium cations are replaced by such metal cations, forming a cross-link between the polymer chains. In this work, the complete bilayer structure was subjected to cross-linking with solutions of salts of bivalent metals, in particular: barium ($Ba(CH_3COOH)_2$, $BaCl_2$), calcium ($Ca(NO_3)_2$, $CaCl_2$) and strontium ($SrCl_2$).

Thus, due to such a set of salts, we can establish correlation between the properties of materials cross-linked with different metal cations but in the presence of the same anion (using chlorides as an example) and materials cross-linked with the same cation but with different salt anions ($BaCl_2$ and $Ba(CH_3COOH)_2$, $CaCl_2$ and $Ca(NO_3)_2$ pairs).

Results

Model samples preparation scheme

Preparation of sodium alginate 2% solution
↓
Addition of surfactant
↓
Step-by-step freezing to -50˚C
↓
Freeze-drying
↓
Cross-linking
↓
Washing off residual salts and alcohol
↓
Step-by-step freezing to -50˚C
↓
Freeze-drying
↓
Applying the film coating
↓
Drying of the top layer at +37˚C

Degradation kinetics of samples (sponges and films separately) using different cross-linking agents

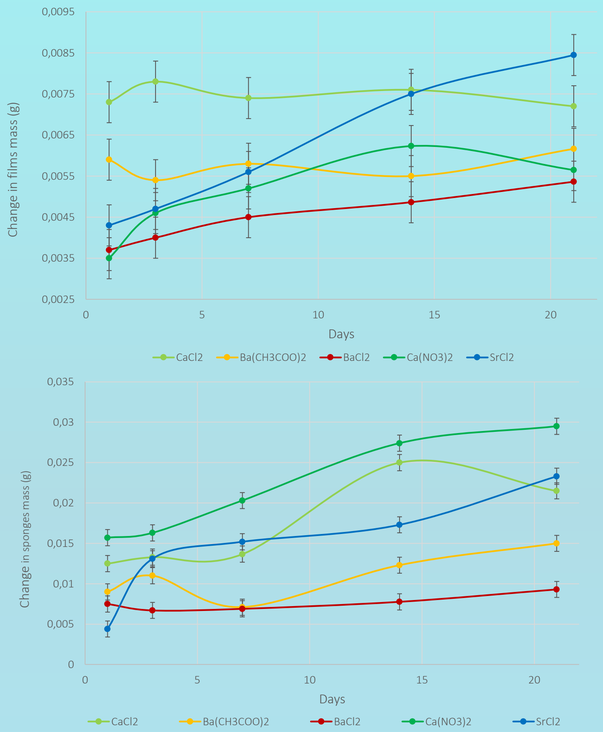

Model samples appearance

Porous layer sample

Double-layered matrix and film coating

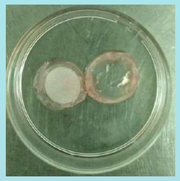

Degradation experiment

Degradation kinetics was assessed in SBF buffer solution simulating extracellular body fluid. The initial mass of the samples was measured to the accuracy of 0.0001 g. Samples were placed in a closed system and it was filled with the buffer solution. The samples were kept in thermostat at 37 ºC for 21 days. The samples were washed thoroughly with distilled water and dried to constant weight, followed by weighing.

Model samples characteristics

Characteristics	Sodium alginate 2%
Deformation limit, %	33,9±0,2
Water vapor transmission rate, g/m²*h	200±8
Tension strength, mPa	5,3±0,4
Porosity, %	94±1
Average pore size, µm	250±15

Scanning electron microscopy of cross-linked porous layer

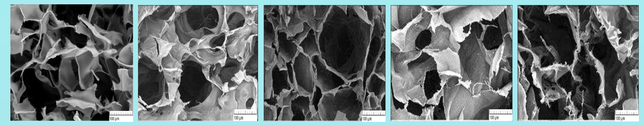

$SrCl_2$ $BaCl_2$ $Ba(CH_3COO)_2$ $Ca(NO_3)_2$ $CaCl_2$

Cross-linking with $BaCl_2$, 20 µm

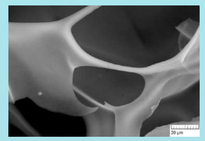

SEM of porous layer without cross-linking

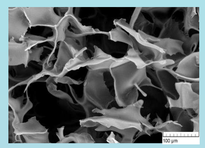

SEM of top layer without cross-linking

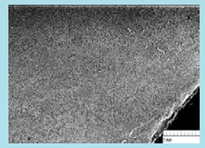

Conclusions

1) The studies showed the possibility of creating a tissue equivalent for dermal regeneration based on sodium alginate with cross-linking agents, in which the surface layer would perform a protective function and the lower layer would improve vascularization and tissue regeneration.
2) Two-layer tissue equivalents based on sodium alginate with porosity of 94%, pore size of 250 nm were developed.
3) Preferred crosslinking salts for sodium alginate to form scaffold structures were determined.
4) It was demonstrated that the pore sizes do not change in dependence on the salts used for cross-linking. A correlation was deduced between the degradation kinetics and the salts used in crosslinking the materials.
5) It was revealed that further studies on the strength of the materials are required.

III International Conference and School
"Synthesis, Structure, and Properties of High-Entropy Materials"
October 11-15, 2021

№ 45

EFFECT OF SWAGING ON IMPACT TOUGHNESS OF AUSTENITIC STAINLESS STEEL

rus.chernichenko@mail.ru

Ruslan Chernichenko [1], Dmitry Panov [1], Stanislav Naumov [1], Nikita Stepanov [1], Gennady Salishchev [1]

[1] Laboratory of Bulk Nanostructured Materials, Belgorod State University, 85 Pobeda Str., 308015 Russian Federation, Belgorod

НИУ БелГУ
BELGOROD STATE UNIVERSITY (BSU)

Introduction

Austenitic stainless steels possess attractive mechanical properties, but low yield strength restricts their applications. Cold swaging is a promising method to increase yield strength [1]. However, some issues of the swaging behavior of the material remain poorly understood. In particular, the effect of the structural gradient formed during swaging on the mechanical properties of the material require further study. Thus, the purpose of this work is to study the effect of swaging on Charpy impact toughness of austenitic stainless steel with a gradient microstructure.

Methods and Materials

TABLE 1. Chemical composition of the program steel

El.	Cr	Ni	Mo	C	P	S	Fe
wt. %	16,82	12,04	1,91	0,1	0,002	0,002	69,12

The program material under study is 316-type austenitic stainless steel. Cold swaging was carried out by swaging with different degrees (20-95% of the initial diameter of the bar), which led to the formation of a microstructural gradient along the bar section.

Conclusion

Cold plastic deformation leads to an increase in dislocation density and initiation of twinning, which resulted in the microstructure fragmentation. The microstructure gradient was observed after swaging. The presence of the structural gradient is also confirmed by measuring Vickers hardness, namely changing the hardness profile from edge to center. After 40% cold swaging, Charpy impact toughness values decrease from 140 J/cm² to ~ 80 J/cm². Further increase of deformation degree is associated with stabilization of Charpy toughness at ~ 60 J/cm².

Results and Discussions

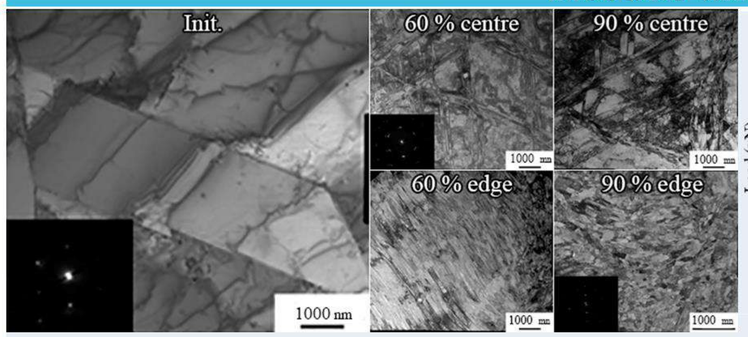

FIGURE 1. TEM-structure of the program steel in (a) the initial state, (b) the center and (c) edge of the bar after cold swaging with 60% reduction, and (d) the center and (e) edge of the bar after cold swaging with 95% reduction.

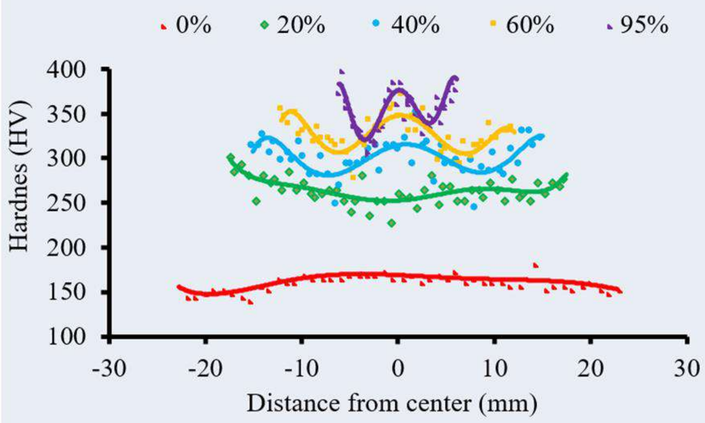

FIGURE 2. (a) Distribution of hardness indices by bar section depending on swaging

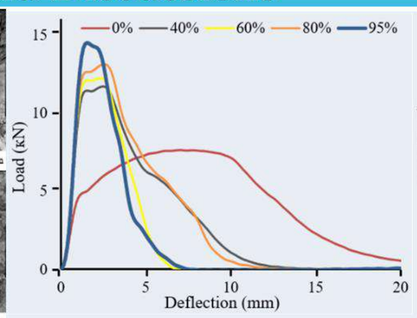

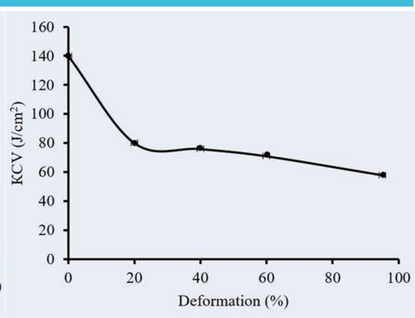

FIGURE 3. (a) Load-deflection plots and (b) dependencies of mechanical properties characteristics after Charpy V-notch impact testing.

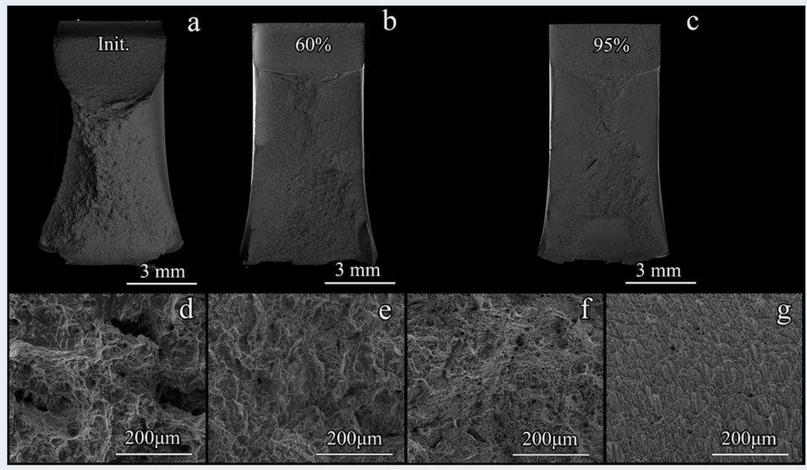

FIGURE 4. (a-c) Fracture overviews and (d-g) SEM-BSE images of fracture in (a, d) the initial state, (b, e) after 60% and 95% (c, f, g) swaging.

TABLE 2. Dynamic parameters of the program steel

Parameters	Deformation, %				
	0%	20%	40%	60%	95%
Stress at yield plateau (σ_{ye}), MPa	463	955	1046	1106	-
Maximum stress (σ_m), MPa	697	1013	1091	1128	1316
Impact plane-strain fracture toughness (K_{Id}), MPa$\sqrt{m}$	107	83	82	72	71

This research was funded by the Russian Science Foundation Grant no. 20-79-10094

III International Conference and School "Synthesis, Structure, and Properties of High-Entropy Materials" October 11-15, 2021

№47

*yuzbekova@bsu.edu.ru

EFFECT OF GRAIN REFINEMENT ON CRYOGENIC BEHAVIOR OF AN AL-MG-SC-ZR ALLOY

Yuzbekova D. Y.*, Mogucheva A. A., Kaibyshev R. O.
Belgorod State National Research University, Belgorod, Russia

The experiments were conducted using an aluminum alloy with a chemical composition of Al-4.57%Mg-0.35%Mn-0.2%Sc-0.09%Zr (wt. pct.)

Microstructure of the AA5024 alloy

Before ECAP

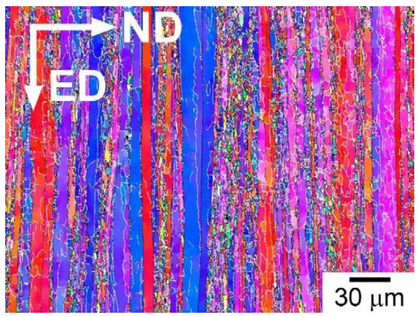

Unrecrystallized structure
d~200/20 μm; ρ~9.8×10^{12} m^{-2}

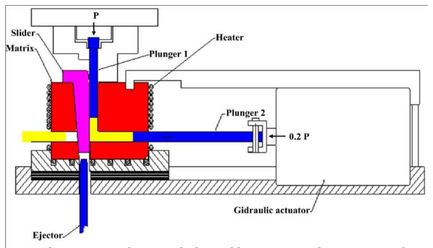

The rods with dimensions of 10×10×110 mm^3 were deformed by ECAP with back pressure at T = 300°C up to ε~12 via route B_c

After ECAP

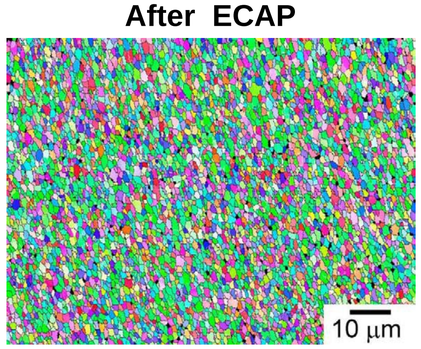

Fully recrystallized structure
d~1 μm; ρ~1.2×10^{14} m^{-2}

Mechanical properties of the AA5024 alloy

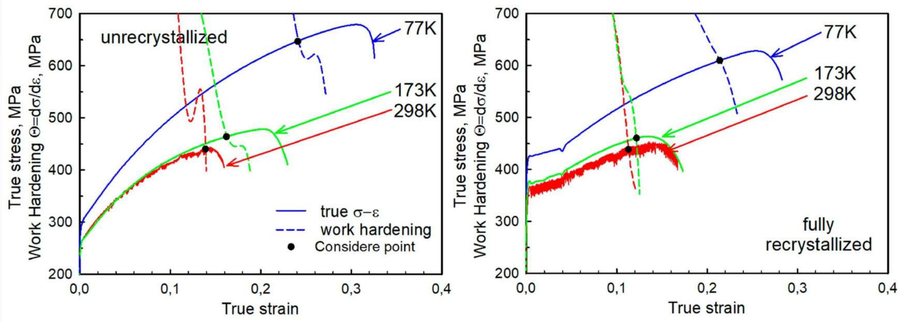

Structural condition	T, K	YS, MPa	UTS, MPa	δ,%	YS_{77K}/YS_{298K}	UTS_{77K}/UTS_{298K}
unrecrystallized	298	260	385	17.3	1.13	1.32
	173	260	395	26.2		
	77	295	510	38.3		
fully recrystallized	298	345	395	18.1	1.22	1.25
	173	370	410	18.9		
	77	420	495	32.7		

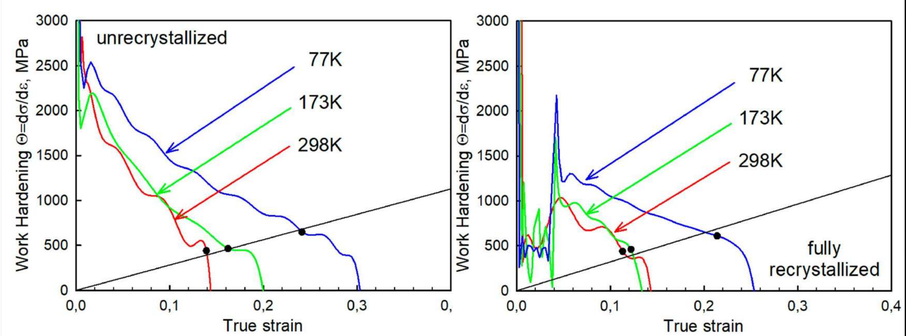

The dislocation density after tension

Structural condition	T=298K $\dot{\varepsilon}$~10^{-3} s^{-1}	T=77K $\dot{\varepsilon}$~10^{-3} s^{-1}
unrecrystallized	1.9×10^{15}	9.1×10^{14}
fully recrystallized	1.2×10^{15}	1.0×10^{15}

Fracture surface of the AA5024 alloy

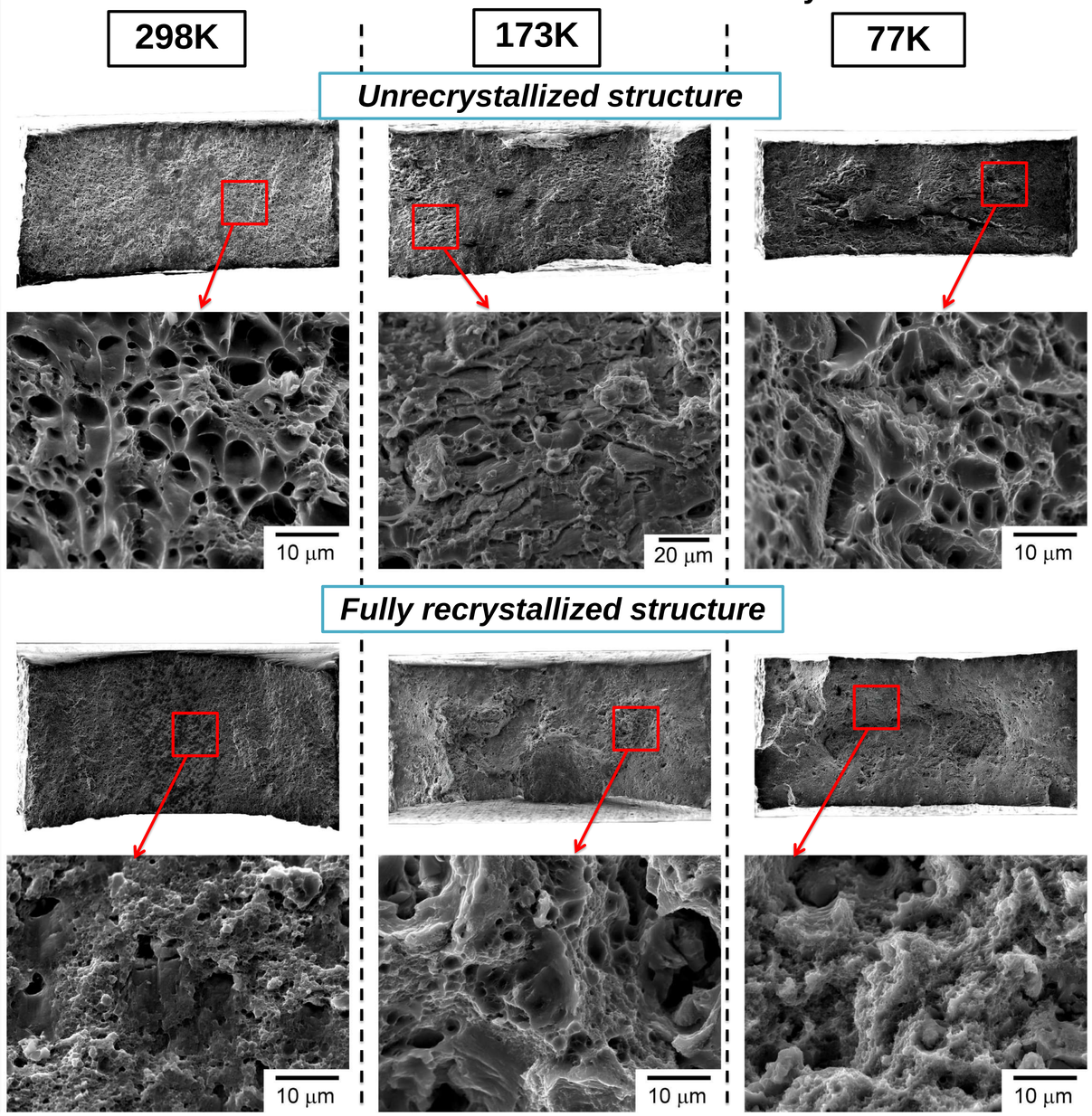

Summary

Grain refinement increases yield stress (YS) probably due to increased contribution of grain boundary strengthening and dislocation strengthening. Continuous yielding takes place in the alloy with unrecrystallized structure, while the formation of fully recrystallized structure leads to transition to discontinuous yielding. The formation of recrystallized structure restrains increment in the elongation-to-failure at cryogenic temperatures due to relatively high YS values of this structural condition that leads to lower work hardening rates. Ductile fracture is the main mechanism of rupture in whole temperature range for both material conditions. The alloy is tough up to cryogenic temperatures and the onset of fracture correlates with the lattice dislocation density attained ~10^{15} m^{-2}.

III International Conference and School
"Synthesis, Structure, and Properties of High-Entropy Materials"
October 11-15, 2021

№ 48

yurchenko_nikita@bsu.edu.ru

YIELD STRENGTH ANOMALY IN A B2 MATRIX AlNbTiVZr$_{0.25}$ REFRACTORY HIGH ENTROPY ALLOY

Yurchenko N.Yu., Panina E.S., Zhilina M.A., Salishchev G.A., Stepanov N.D.

The vast compositional space of the recently introduced high entropy alloys (HEAs) concept offers new horizons in tuning the properties of intermetallics and their formation in unexpected systems . For instance, unable to appear in binary Al-ETM (ETM-early transition metal) system, an Al-containing B2 phase becomes stable in refractory high entropy alloys (RHEAs), which are new potential high-temperature materials. In RHEAs, the B2 phase can play the role of either matrix or secondary phase, replicating the successful microstructure design of nickel-based superalloys. However, many aspects of the mechanical behaviour and deformation mechanisms of the multicomponent B2 phase in RHEAs remain unexplored. One such feature is yield strength anomaly (YSA). YSA is a positive temperature dependence of strength, which is typical for some materials, including B2 compounds . This study evidenced the YSA in a B2 matrix AlNbTiVZr$_{0.25}$ RHEA in the temperature interval of 600-800°C.

Initial structure (annealing at 1200°C, 24 h)

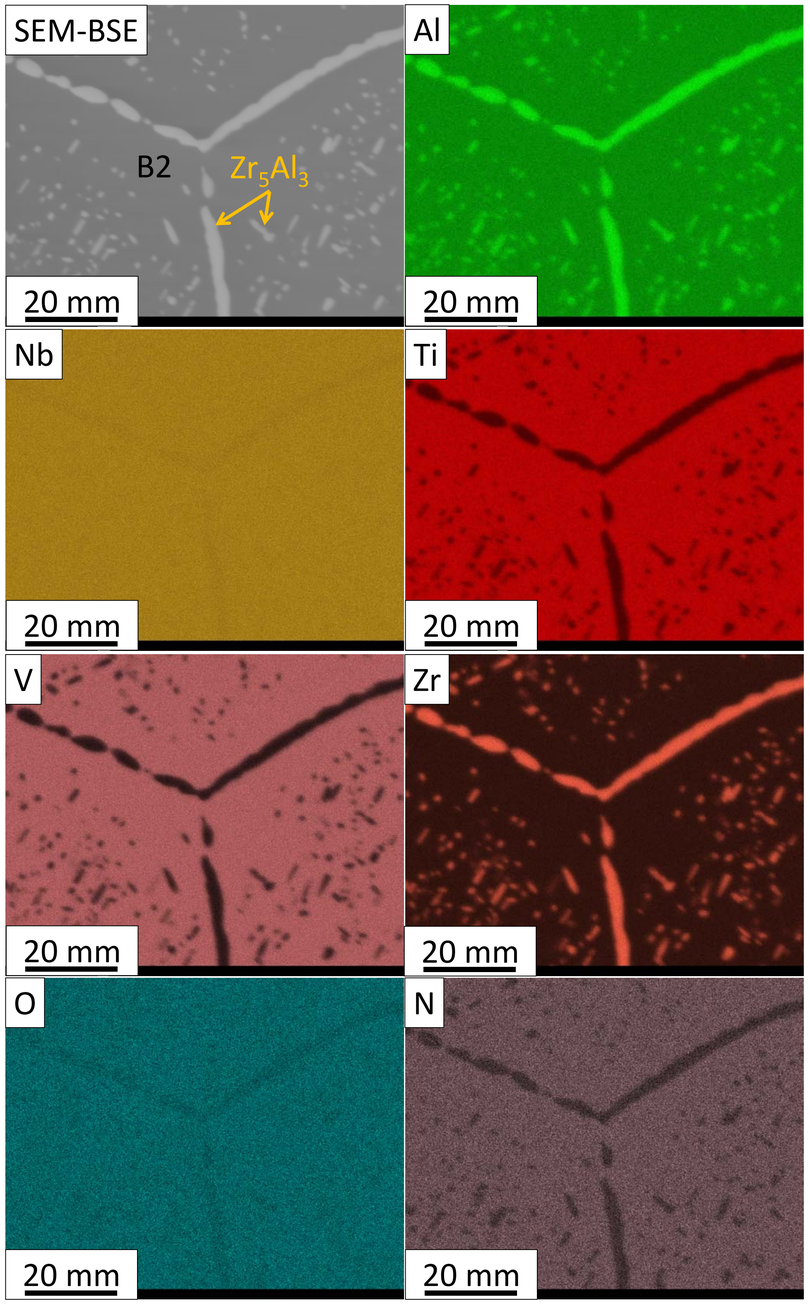

Compression test, strain rate = 10^{-4} s^{-1}

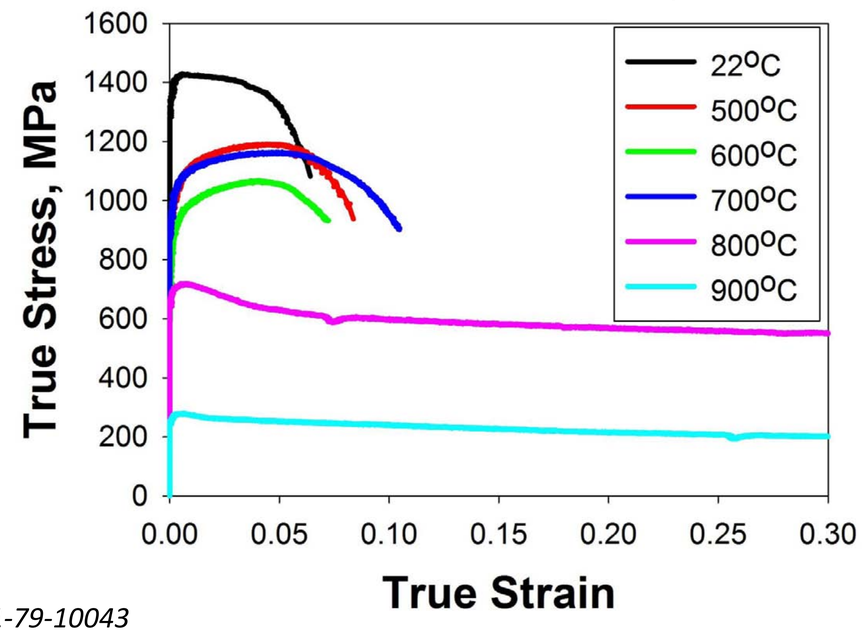

Yield strength anomaly

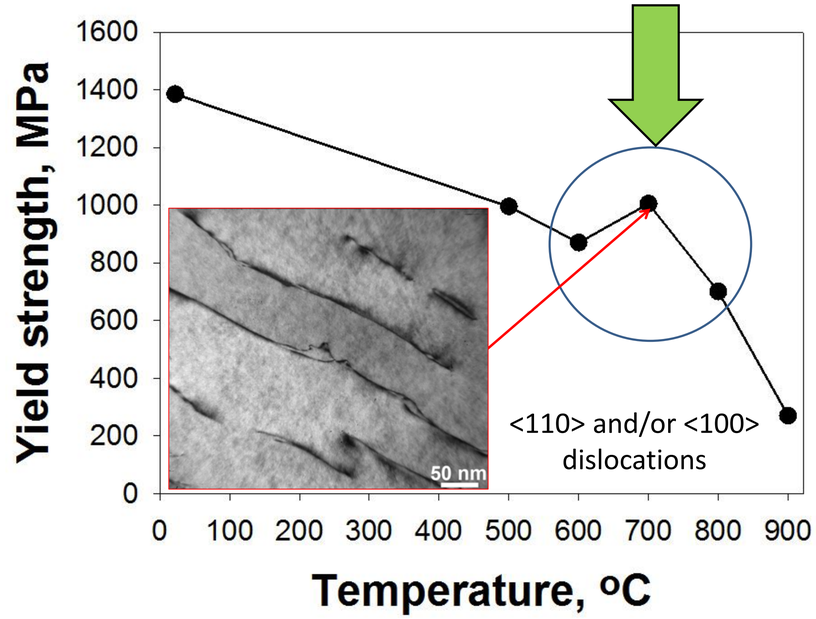

This study was supported by Russian Science Foundation, grant № 21-79-10043

E-mail:
alena_novoselova@list.ru

III International Conference and School
"Synthesis, Structure, and Properties of High-Entropy Materials"
October 11-15, 2021

SYNTHESIS AND THERMODYNAMICS OF DOUBLE Dy-Ga AND TRIPLE Dy-Ga-Al, Pr-Ga-In ALLOYS IN MOLTEN SALT-LIQUID METAL SYSTEMS

Alena Novoselova, Valeri Smolenski

Institute of High-Temperature Electrochemistry Russian Academy of Science, Ekaterinburg, Russia

Currently, rare earth based alloys are essential and very important for various branches of industries, primarily in metallurgy, electronics, nuclear power, and in the production of catalysts, magnetic materials, etc. Electrochemical processes for the production of metal alloys in the "molten salt-liquid metal" systems allow to obtain the necessary compounds with the specified properties with a sufficiently high efficiency. The goal of this research was to study the reaction of the cathode formation of the alloys, the conditions for its production in molten salt media and calculation of its thermodynamic characteristics.

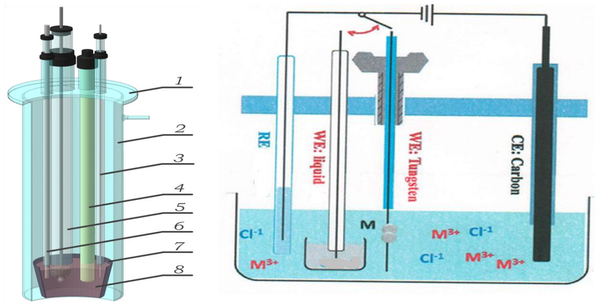

Fig. 1 Electrochemical cell for investigations

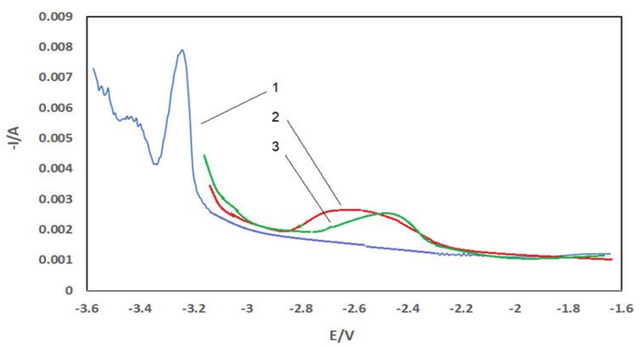

Fig. 2 SWV of LiCl-KCl-CsCl-DyCl3 molten salt solution

Square wave voltammetry were used to establish the reaction of electrochemical reduction of Ln(III) ions in different molten salts on inert and active electrodes. The shift of the dysprosium or praseodymium potentials deposition peak to the electropositive region on the active electrodes by comparison with inert ones can be associated with the process of alloy formation. XRD pattern of the samples obtained on different active electrodes after electrolysis showed the formation of the intermetallic compounds of different composition. The reaction of alloy formation can be written by the following scheme:

$$x[LnCl_6]^{3-} + 3\bar{e} + y(Me_1 + Me_2) = Ln_x(Me_1 + Me_2)_y + 6xCl^-$$

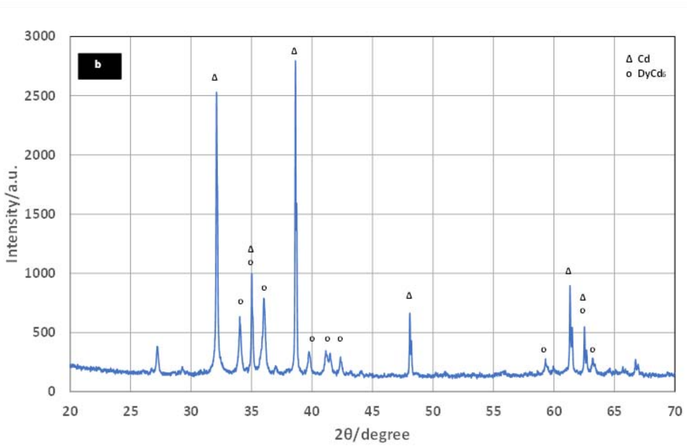

Fig. 3 XRD pattern of Dy-Cd intermetallic compound

Table 1. Activity coefficients of Pr in liquid bimetallic Ga-In alloys

T/K	$\log\gamma_{Pr-Ga}$ Pr-Ga	$\log\gamma_{Pr(Ga-In)}$ Pr-Ga-20 wt.% In	$\log\gamma_{Pr(Ga-In)}$ Pr-Ga-40 wt.% In	$\log\gamma_{Pr(Ga-In)}$ Pr-Ga-70 wt.% In	$\log\gamma_{Pr-In}$ Pr-In
723	-14.46	-13.88	-13.03	-12.04	-10.50
751	-13.79	-13.19	-12.40	-11.33	-9.98
779	-13.18	-12.69	-11.84	-10.95	-9.50
872	-11.42	-10.88	-10.09	-9.34	-8.13
938	-10.38	-9.96	-9.17	-8.41	-7.32
1001	-9.52	-9.07	-8.35	-7.61	-6.65
1067	-8.72	-8.85	-7.59	-6.93	-6.03

- **The conditions for production of alloys of different composition were determined.**
- **The principle thermodynamic properties of dysprosium and praseodymium in various alloys were calculated.**

The research was carried out with the financial support of the RFBR in the framework of scientific project No. 20-03-00743.

The following galvanic cells were used for measuring the equilibrium electrode potentials of the alloys by open-circuit potentiometry (OCP):

(-) $Dy(Ga)_{(dilute\ sol.)}$ | electrolyte ‖solvent | $C_{(s)}, Cl_{2(g)}$ (+)
(-) $Dy(Ga\text{-}Al)_{(dilute\ sol.)}$ | electrolyte ‖solvent | $C_{(s)}, Cl_{2(g)}$ (+)
(-) $Pr(Ga\text{-}In)_{(dilute\ sol.)}$ | electrolyte ‖solvent | $C_{(s)}, Cl_{2(g)}$ (+)

Dysprosium and praseodymium dilute solutions of Dy-Ga, Dy-Ga-Al and Pr-Ga-In alloys were prepared by electrolysis of different molten salts directly in the electrochemical cell before the experiments.

For calculation of the thermodynamic characteristics of the alloy formation processes open-circuit potentiometry were used. The value of the partial excess Gibbs free energy change of Dy or Pr in liquid alloys of different composition was calculated:

$$\Delta G^{ex}_{Dy(Ga)} = -195.4 + 0.081 \cdot T \pm 2.8 \quad kJ/mol \qquad (LiCl\text{-}KCl)_{eut}$$

$$\Delta G^{ex}_{Dy(Ga-20wt.\%\ Al)} = -201.5 + 0.078 \cdot T \pm 2.8 \quad kJ/mol \qquad (LiCl\text{-}KCl)_{eut.}$$

$$\Delta G^{ex}_{Pr(Ga-20wt.\%\ In)} = -243.8 + 0.072 \cdot T \pm 3.6 \quad kJ/mol \qquad (LiCl\text{-}KCl\text{-}CsCl)_{eut.}$$

$$\Delta G^{ex}_{Pr(Ga-40wt.\%\ In)} = -232.9 + 0.075 \cdot T \pm 3.1 \quad kJ/mol \qquad (LiCl\text{-}KCl\text{-}CsCl)_{eut}$$

$$\Delta G^{ex}_{Pr(Ga-70wt.\%\ In)} = -215.9 + 0.071 \cdot T \pm 3.9 \quad kJ/mo \qquad (LiCl\text{-}KCl\text{-}CsCl)_{eut.}$$

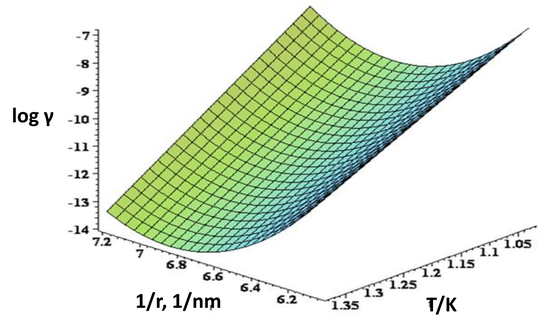

Fig. 4 Three-dimensional graph of log γ – 1/r – T in fused Pr-Ga-In/LiCl-KCl-CsCl system

III International Conference and School
"Synthesis, Structure, and Properties of High-Entropy Materials"
October 11-15, 2021

№ 52

pervikov@list.ru

Institute of Strength Physics and Materials Science Siberian Branch of Russian Academy of Sciences, Tomsk, Russia

Pervikov A.V., Suliz K.V.

OBTAINING OF HEA NANOPARTICLES BY JOINT ELECTRIC EXPLOSION OF WIRES FROM DISSIMILAR METALS/ALLOYS

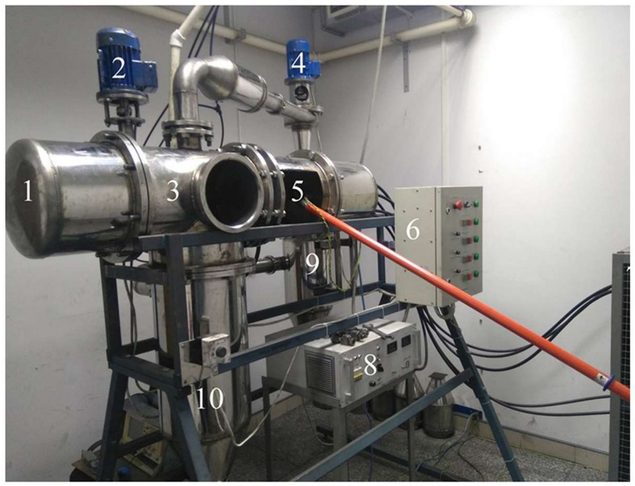

Metals	c, % mol.
Fe	23
Cu	31
Al	14
Ni80Cr20	Ni – 25, Cr – 7

AlNiCrFeCu		
δ	$100\% \times \sqrt{\sum_{i=1}^{n} c_i \left(1 - \frac{r_i}{\sum_{j=1}^{n} c_j \cdot r_j}\right)^2}$	4,91 %
ΔH_{mix}	$\sum_{i=1, i\neq j}^{n} 4 \cdot \Delta H_{mix} \cdot c_i \cdot c_j$	-0,17 кДж/моль
ΔS_{mix}	$-R \sum_{i=1}^{n} c_i \cdot \ln c_i$	12,54 Дж/К/моль
VEC	$\sum_{i=1}^{n} c_i (VEC)_i$	8

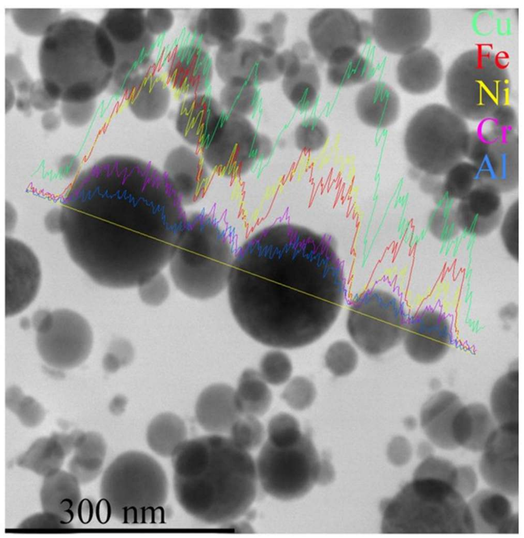

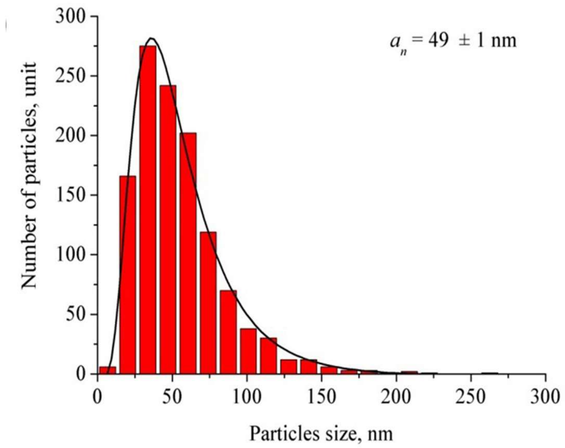

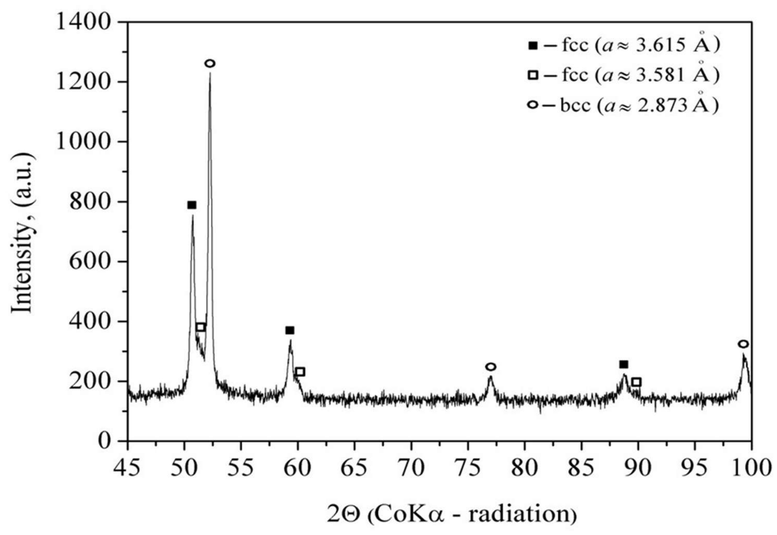

III International Conference and School
"Synthesis, Structure, and Properties of High-Entropy Materials"
October 11-15, 2021

№ 53

E-mail kurbellya@mail.ru

THERMAL STABILITY IN MULTICOMPONENT ALLOYS BASED ON D METALS

Kurbanova E.D., Polukhin V.A.

Institute of Metallurgy of the Ural Branch of the Russian Academy of Sciences Ekaterinburg, Russia

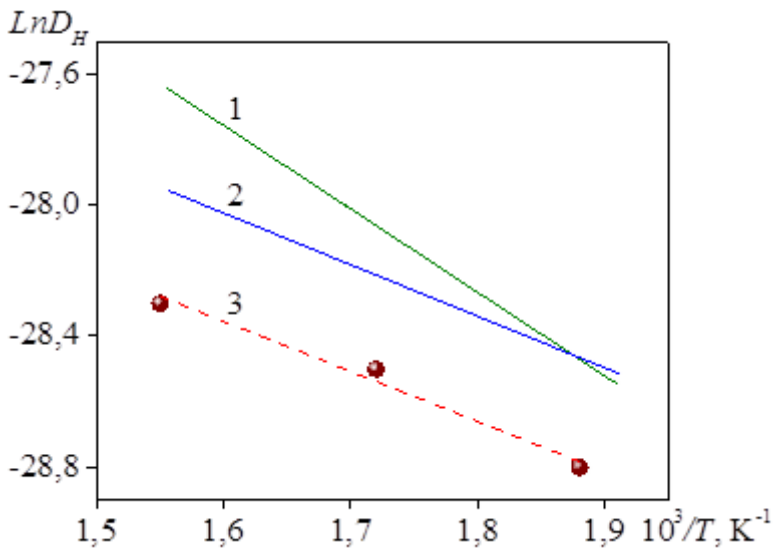

a

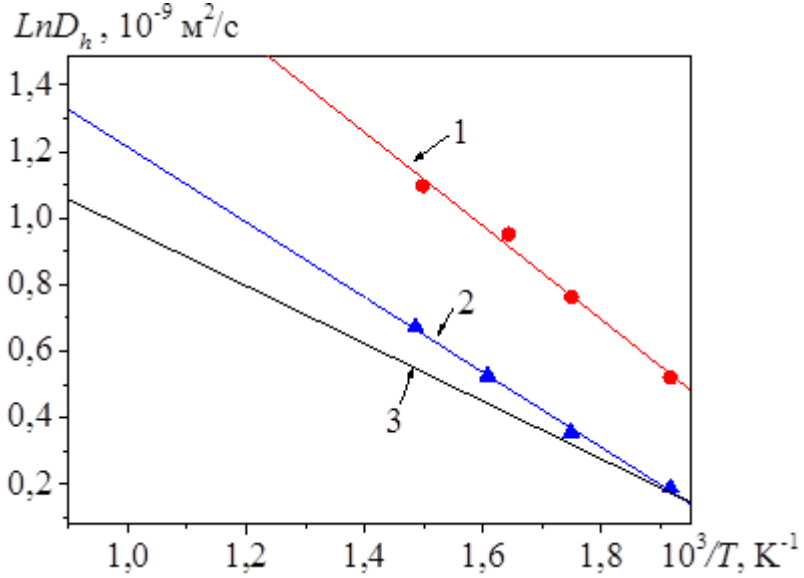

b

Experimental, calculated (according to the Arrhenius law and MD simulation of diffusion, DH with a logarithmic dependence of hydrogen diffusion on the reciprocal temperature for alloys: a) –Fe40Ni38B18Mo4 in the amorphous state (curve 1) and in the nanocrystalline state (curve 2) under conditions: pressure P=1MPa and temperatures from 523 to 643 K [1]. Curve 3 - theoretical calculation of MD simulation; b) Temperature dependences of averaged diffusion of hydrogen DH, presented for different alloys (marked by arrows), 1 - crystalline, curve Nb40-xMoxTi30Ni30 (x=5, 10), 673 K - operating temperature with activation energy (Ea=24.2 kJ/mol); 2 and 3 - nanocrystalline alloy – Nb70-xTixNi30 (x=30), Ea=24.22 kJ / mol, respectively, experimental and calculated MD.

The work was carried out under the State Assignment of the IMET UB RAS in the framework of the Program of Fundamental Research of State Academies (topic 19-2)

1. Polukhin V.A., Sidorov N.I., Vatolin N.A. Presolidification changes in the structural–dynamic characteristics of glass-forming metallic melts during deep cooling, vitrification, and hydrogenation, Russian Metallurgy (Metally), 2019, vol. 2019, issue 8, p. 758-780. DOI: 10.1134/S0036029519080123.